THE UNIVERSITY OF ALABAMA® | University Libraries

An Iterative Learning Controller for a Switched Cooperative Allocation Strategy During Sit-to-Stand Tasks with a Hybrid Exoskeleton

Vahidreza Molazadeh – National Institutes of Health Clinical Center
Qiang Zhang – NC State University
Xuefeng Bao – Case Western Reserve University
Nitin Sharma – NC State University

Deposited 01/08/2025

This is an accepted manuscript from the journal IEEE Transactions on Control Systems and Technology in 2022 available at: doi: 10.1109/TCST.2021.3089885.

Citation of published version:

V. Molazadeh, Q. Zhang, X. Bao and N. Sharma, "An Iterative Learning Controller for a Switched Cooperative Allocation Strategy During Sit-to-Stand Tasks with a Hybrid Exoskeleton," in *IEEE Transactions on Control Systems Technology*, vol. 30, no. 3, pp. 1021-1036, May 2022, doi: 10.1109/TCST.2021.3089885.

© 2022 IEEE. This work is licensed under a CC BY-NC 4.0 license.

An Iterative Learning Controller for a Switched Cooperative Allocation Strategy During Sit-to-Stand Tasks with a Hybrid Exoskeleton

Vahidreza Molazadeh, Qiang Zhang, Xuefeng Bao, *Member, IEEE*, and Nitin Sharma, *Senior Member, IEEE*

***Abstract*— A hybrid exoskeleton that combines functional electrical stimulation (FES) and a powered exoskeleton is an emerging technology for assisting people with mobility disorders. The cooperative use of FES and the exoskeleton allows active muscle contractions through FES while robustifying torque generation to reduce FES-induced muscle fatigue. In this article, a switched distribution of allocation ratios between FES and electric motors in a closed-loop adaptive control design is explored for the first time. The new controller uses an iterative learning neural network (NN)-based control law to compensate for structured and unstructured parametric uncertainties in the hybrid exoskeleton model. A discrete Lyapunov-like stability analysis that uses a common energy function proves asymptotic stability for the switched system with iterative learning update laws. Five human participants, including a person with complete spinal cord injury, performed sit-to-stand tasks with the new controller. The experimental results showed that the synthesized controller, in a few iterations, reduced the root mean square error between desired positions and actual positions of the knee and hip joints by 46.20% and 53.34%, respectively. The sit-to-stand experimental results also show that the proposed NN-based iterative learning control (NNILC) approach can recover the asymptotically trajectory tracking performance despite the switching of allocation levels between FES and electric motor. Compared to a proportional-derivative controller and traditional iterative learning control, the findings showed that the new controller can potentially simplify the clinical implementation of the hybrid exoskeleton with minimal parameters tuning.**

Manuscript received December 1, 2020; revised April 18, 2021; accepted June 4, 2021. Date of publication July 5, 2021; date of current version April 12, 2022. This work was supported in part by the National Science Foundation (NSF) under Award 1646009. Recommended by Associate Editor M. Maggiore. *(Corresponding author: Nitin Sharma.)*

This work involved human subjects or animals in its research. Approval of all ethical and experimental procedures and protocols was granted by the Institutional Review Board (IRB) at the University of Pittsburgh under Approval No. PRO14040419 and the North Carolina State University under IRB Approval No. 20533.

Vahidreza Molazadeh is with the Rehabilitation Medicine Department, Functional and Applied Biomechanics Section, National Institutes of Health Clinical Center, Bethesda, MD 20892 USA (e-mail: vahidreza.molazadeh@nih.gov).

Qiang Zhang and Nitin Sharma are with the Joint Department of Biomedical Engineering, North Carolina State University, Raleigh, NC 27695 USA, and also with the Joint Department of Biomedical Engineering, University of North Carolina Chapel-Hill, Raleigh, NC 27599 USA (e-mail: qzhang25@ncsu.edu; nsharm23@ncsu.edu).

Xuefeng Bao is with the Department of Biomedical Engineering, Case Western Reserve University, Cleveland, OH 44106 USA (e-mail: xub3@pitt.edu).

Color versions of one or more figures in this article are available at https://doi.org/10.1109/TCST.2021.3089885.

Digital Object Identifier 10.1109/TCST.2021.3089885

***Index Terms*— Functional electrical stimulation (FES), hybrid exoskeleton, iterative learning control, neural networks (NNs), powered exoskeleton, virtual constraints.**

I. Introduction

NEUROLOGICAL injuries such as stroke and spinal cord injury (SCI) impede standing and walking activities, causing significant mobility challenges for people with these disorders. Functional electrical stimulation (FES) is a potential technology to restore standing and walking functions. FES was used for the first time in the 1960s by Kantrowitz [1] and Liberson *et al.* [2] to correct drop foot. Since then, FES has been used for restoring more complex human lower limb functions such as walking [3], [4] and standing up [5]–[9]. FES enables active muscle contractions, which promotes its therapeutic benefits such as increasing metabolic energy consumption, increasing neuroplasticity [10], improving cardiovascular fitness, preventing muscle atrophy, and increasing bone density [11]. Despite the progress made in the field of FES and its benefits, the rapid onset of FES-induced muscle fatigue remains a major technical hurdle because the consequent reduction in muscle force limits the duration of sit-to-stand and walking activities.

A powered exoskeleton is an alternative rehabilitation technology for enabling people with paraplegia caused by SCI to regain lower limb functions [12]–[17]. However, unlike FES, which elicits active muscle contractions, the powered exoskeleton passively enables limb movements. Additionally, current powered exoskeletons need considerable battery power because of high energy consumption during walking, limiting their portability.

Hybrid exoskeletons that combine a powered exoskeleton with an FES system exploit each technology's benefits and overcome their shortcomings [18]–[20]. A hybrid exoskeleton can offset FES-induced fatigue effects that reduce muscles' force-generation capability. Furthermore, the use of FES can potentially reduce actuator size and battery usage and thus increase the hybrid device's portability [18], [19], [21]–[24].

A cooperative strategy is a hybrid exoskeleton control approach where both FES and the exoskeleton contribute to the desired joint torque. Recent powered exoskeleton control techniques such as model-based feedback linearization [25] and Jacobian linearization [15], when used in the hybrid exoskeleton, may not guarantee exponential convergence. This

technical challenge is primarily because of the presence of modeling uncertainties in the FES-driven musculoskeletal system. Because of the day-to-day variations and interperson variations in the musculoskeletal modeling parameters and the tedious process needed to identify the musculoskeletal model [20], clinical implementation of model-based controllers is nontrivial. Model-based approaches may be combined with an adaptive or robust term for coordinating FES and the exoskeleton. In [21], a cooperative and adaptive muscle control loop simultaneously controlled stimulation of the hamstrings and quadriceps muscles and the hip and knee electric motors during level walking. The muscle control loop utilized joint torque profiles from previous steps to shape the subsequent steps' muscle stimulation profiles. In [26], the control strategy combined a proportional-integral-derivative (PID) controller for an active lower limb exoskeleton with an event-based FES stimulation trigger during the extension subphase to cooperatively produce substantial assistive torque.

Unlike the approaches in [19], [21], and [26], our previous work focused on incorporating muscle fatigue dynamics in the cooperative control design. A nonlinear model predictive controller was used to optimize coordination between FES and an electric motor during a knee joint control task [20]. A desired allocation ratio distributed the joint limb torque between FES and the electric motor. An update strategy would change the allocation ratio based on the fatigue dynamics while regulating a desired knee joint angle. For example, the allocation ratio is set as 1 (FES): 0 (motor) when the muscle is not fatigued and 0 (FES): 1 (motor) when the muscle is fully fatigued, with intermediate allocation values in between. However, this approach was limited to a single joint and was not robust to modeling uncertainties. In [22], [23], and [27], a muscle synergy-inspired controller used a set of synergy blocks to control different muscle groups and multiple electric motors during walking or swing-like leg movements. Each synergy acted as a set of allocation ratios for different actuators. A robust adaptive term modified the coefficients of a combination of synergies to compensate for the muscle fatigue, and a modified PD controller provided robustness to modeling uncertainties.

The muscle synergy-inspired controllers in [22], [23], and [27] enable automatic allocation of effort between FES and the powered exoskeleton and have been shown to provide good performance. However, their control design may not guarantee desired joint torque levels or system stability if the control allocation ratios are manually switched. In some situations, a therapist/clinician may prefer a switched manual allocation ratio between FES and the electric motor. For example, a therapist/clinician may choose an appropriate training mode of the hybrid exoskeleton for patients at different rehabilitation training stages or different muscle fatigue levels. The novel control method developed in this article enables a therapist/clinician to train a patient in different training modes and lets them arbitrarily switch the allocation ratio without fear of device instability. Therefore, we propose a cooperative control strategy that can handle the arbitrarily switched allocation ratios between FES and electric motor. The predetermined allocation ratios can be switched arbitrarily based on an external command or a fatigue-based update strategy. The proposed controller also uses virtual constraint-inspired desired trajectories. Virtual constraints are time-invariant profiles that were originally used for bipedal robots as reference trajectories in [28] and [29] and have recently been used for wearable robot control [25], [30]–[32].

This article's main contribution is the design of a unique adaptive cooperative control framework that distributes a top-level torque between FES and the electric motor through allocation coefficients that can be manually switched during a sit-to-stand task with multiple DOF hybrid exoskeletons. Unlike our previous work on torque allocation between FES and the electric motor, where full or partial model knowledge was required for control design [20], [22], [23], [27], the novel proposed control method can learn unknown system dynamics for a repeated sit-to-stand task by using a neural network (NN) control design in an iterative learning control (ILC) framework. ILC is especially helpful to achieve good trajectory performance in repetitive rehabilitation tasks [33]–[35]. NN-based controllers have been extensively investigated for nonlinear control systems with unstructured dynamics or modeling uncertainties [36], [37]. The proposed novel NN-based ILC method can learn parametric uncertainties, including not linearly parameterizable and highly nonlinear terms, by choosing a suitable number of neurons and NN layers. There are two NNs in the proposed controller. The first NN compensates for the unstructured nonlinear terms in the system dynamics, and the second NN compensates for the unknown input distribution matrix for FES input. A discrete Lyapunov-like stability analysis proves asymptotic stability for the adaptive switched system with iteratively learning update laws. To the best of the authors' knowledge, a switched distribution of control allocation ratios in a closed-loop adaptive control design is currently unexplored for hybrid exoskeleton control. Additionally, it is unknown whether a traditional continuous Lyapunov function candidate would facilitate stability analysis of the arbitrarily switched allocation ratios. Compared to our previous work in [38] and [39], this article presents a more detailed controller derivation, stability analysis, and extensive experiments with a hybrid exoskeleton on five participants (including a patient with complete spinal cord injury) for a sit-to-stand task. Furthermore, the proposed NN-based ILC method's effectiveness and advantages are evaluated through the experimental comparison study to traditional proportional-derivative control and a pure ILC method.

II. General Hybrid Exoskeleton Lower Limb Model

The dynamics of a general N degrees of freedom (N-DOF) hybrid exoskeleton can be written as

$$\boldsymbol{M}(\boldsymbol{q})\ddot{\boldsymbol{q}} + \boldsymbol{C}(\boldsymbol{q}, \dot{\boldsymbol{q}})\dot{\boldsymbol{q}} + \boldsymbol{G}(\boldsymbol{q}) + \boldsymbol{\tau}_p = \boldsymbol{\tau}_{\text{in}} \tag{1}$$

where $\boldsymbol{q} \in \mathbb{R}^N$ is defined as $\boldsymbol{q} = [\theta_1, \theta_2, \ldots, \theta_N]^T$. θ_i ($i = 1, 2, \ldots, N$) is the angular position of the ith linkage. $\boldsymbol{C}(\boldsymbol{q}, \dot{\boldsymbol{q}}) \in \mathbb{R}^{N\times N}$ is the Centripetal-Coriolis matrix, $\boldsymbol{M}(\boldsymbol{q}) \in \mathbb{R}^{N\times N}$ is the inertia matrix, $\boldsymbol{G}(\boldsymbol{q}) \in \mathbb{R}^N$ is the gravitational vector, and

$$\boldsymbol{\tau}_{\text{in}} = \boldsymbol{B}_E(\boldsymbol{q}, \dot{\boldsymbol{q}})\boldsymbol{u}_E + \boldsymbol{B}_M\boldsymbol{u}_M \tag{2}$$

where $\boldsymbol{B}_E(\boldsymbol{q}, \dot{\boldsymbol{q}}) \in \mathbb{R}^{N\times N}$ is the FES input distribution matrix [22], [23], [27], $\boldsymbol{B}_M \in \mathbb{R}^{N\times N}$ is the powered motor

input distribution matrix [22], [23], [27], $\boldsymbol{u}_E \in \mathbb{R}^N$ is the normalized muscle stimulation, and $\boldsymbol{u}_M \in \mathbb{R}^N$ is the motor torque input. In (1), $\boldsymbol{\tau}_\mathbf{p} \in \mathbb{R}^N$ is the passive moment of the targeted joint caused by the viscosity and elasticity of the targeted muscles. Detailed definitions of $\boldsymbol{B}_E$, $\boldsymbol{B}_M$, and $\boldsymbol{\tau}_\mathbf{p}$ are in [20], [22], [23], [27]. The dynamics in (1) can be rewritten in state space form as

$$\dot{\boldsymbol{x}} = f(\boldsymbol{x}) + \boldsymbol{g}_E(\boldsymbol{x})\boldsymbol{u}_E + \boldsymbol{g}_M(\boldsymbol{x})\boldsymbol{u}_M \tag{3}$$

where $\boldsymbol{x} = \left[\boldsymbol{q}^T, \dot{\boldsymbol{q}}^T\right]^T$. $\boldsymbol{f}(\boldsymbol{x})$, $\boldsymbol{g}_E(\boldsymbol{x})$, and $\boldsymbol{g}_M(\boldsymbol{x})$ are given as the following expressions, respectively,

$$\boldsymbol{f}(\boldsymbol{x}) = \begin{bmatrix} \boldsymbol{I}_{N\times N}\dot{\boldsymbol{q}} \\ \boldsymbol{M}(\boldsymbol{q})^{-1}(\boldsymbol{\tau}_p - \boldsymbol{G}(\boldsymbol{q}) - \boldsymbol{C}(\boldsymbol{q},\dot{\boldsymbol{q}})\dot{\boldsymbol{q}}) \end{bmatrix},$$
$$\boldsymbol{g}_E(\boldsymbol{x}) = \begin{bmatrix} \boldsymbol{0}_{N\times N} \\ \boldsymbol{M}(\boldsymbol{q})^{-1}\boldsymbol{B}_E(\boldsymbol{q},\dot{\boldsymbol{q}}) \end{bmatrix},$$
$$\boldsymbol{g}_M(\boldsymbol{x}) = \begin{bmatrix} \boldsymbol{0}_{N\times N} \\ \boldsymbol{M}(\boldsymbol{q})^{-1}\boldsymbol{B}_M \end{bmatrix}.$$

III. Movement Profile Design and Optimization

A sit-to-stand movement profile is designed offline through an optimization process. The desired profile is used later during the controller implementation. In the optimization process, a hybrid exoskeleton movement is simulated in a closed-loop control scheme with various virtual constraint candidates [29]. The details of the optimization process are provided hereafter.

Define $h_d(\theta(\boldsymbol{q})) \in \mathbb{R}^N$ as a desired virtual constraint function that is represented with the Bezier polynomials given follows:

$$h_d(\theta(\boldsymbol{q})) = \begin{bmatrix} b_1(w(\boldsymbol{q})) \\ b_2(w(\boldsymbol{q})) \\ \vdots \\ b_N(w(\boldsymbol{q})) \end{bmatrix} \tag{4}$$

where

$$b_i(w) = \sum_{k=0}^{M} \varrho_k \frac{M!}{k!(M-k)!} w^k (1-w)^{M-k}. \tag{5}$$

In (5) $M \in \mathbb{Z}$ is the number of Bezier polynomial terms, ϱ_k is the parameter that is determined through optimization, and w is calculated according to the following equation:

$$w(\boldsymbol{q}) = \frac{\theta(\boldsymbol{q}) - \theta^+}{\theta^- - \theta^+} \tag{6}$$

where θ^+ and θ^- are the maximum and minimum values of $\theta(\boldsymbol{q})$, respectively, and $\theta(\boldsymbol{q}) = \zeta_1\theta_1 + \zeta_2\theta_2 + \cdots + \zeta_N\theta_N$. $\zeta_i \in \mathbb{R}$ $(i = 1, 2, \ldots, N)$ is elaborately chosen such that the phase variable, $\theta(\boldsymbol{q})$ is monotonically increasing (or monotonically decreasing). In this article, a sit-to-stand task is chosen for investigating the performance of the controller. For the sit-to-stand task, it is common that the knee joints' trajectories change monotonically, either increasing or decreasing, based on a chosen coordinate. Therefore, both the right or left knee joint angle could be selected as the phase variable. Each leg cannot have an independent phase variable because it causes miscoordination and misalignment between the right and left legs. Therefore, in this article, we only selected the right knee joint angle as the phase variable to coordinate both legs' joints.

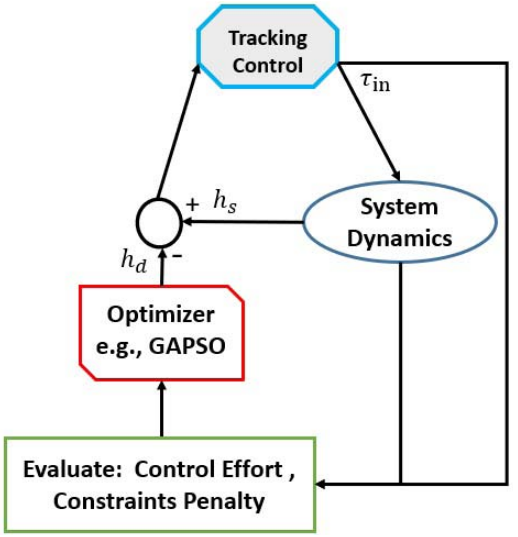

Fig. 1. Flow chart of the virtual constraints optimization.

Additionally, because all joints, including the right knee, are actuated, one of the joints (here the right knee) follows a predesigned time-dependent trajectory. All other joints use the actual right knee angle (not the desired right knee angle) as the phase variable. It should also be noted that the right knee desired velocity is also a function of the right knee phase variable.

To obtain an optimal movement, the value of ϱ_k in the Bezier polynomials in (5) can be determined using a GAPSO optimization algorithm [40]. The following cost function is defined based on the minimum control effort criteria:

$$\begin{aligned} \min_{\varrho_k} J &= \frac{1}{2L}\int_0^{t_f} \boldsymbol{\tau}_{in}^T \boldsymbol{\tau}_{in} dt \\ &+ \frac{1}{2}\left[h_s\left(\boldsymbol{q}_{d_f}\right) - h_d\left(\theta\left(\boldsymbol{q}_{t_f}\right)\right)\right]^T \\ &\boldsymbol{P}\left[h_s\left(\boldsymbol{q}_{d_f}\right) - h_d\left(\theta\left(\boldsymbol{q}_{t_f}\right)\right)\right] \\ \text{s.t.}\quad & \boldsymbol{M}(\boldsymbol{q})\ddot{\boldsymbol{q}} + \boldsymbol{C}(\boldsymbol{q},\dot{\boldsymbol{q}})\dot{\boldsymbol{q}} + \boldsymbol{G}(\boldsymbol{q}) + \boldsymbol{\tau}_\mathbf{p} = \boldsymbol{\tau}_\mathbf{in} \end{aligned} \tag{7}$$

where t_f is the standing duration time, L is a normalizing constant, $h_s\left(\boldsymbol{q}_{d_f}\right) \in \mathbb{R}^N$ is an independent joint angle function, $\boldsymbol{P} \in \mathbb{R}^{N\times N}$ is a weight matrix, $\boldsymbol{q}_{d_f}$ is the vector of the desired final conditions, and $\boldsymbol{q}_{t_f}$ is the vector of the final standing angular positions. The flowchart in Fig. 1 shows the optimization process.

IV. Controller Design

In this section, a robust NN-based iterative learning control (NNILC) method with the consideration of the arbitrarily switched allocation ratios between FES and exoskeleton motors is designed. First, the output error term $\boldsymbol{e} \in \mathbb{R}^N$ is defined as

$$\boldsymbol{e} = h(\boldsymbol{q}) = h_s(\boldsymbol{q}) - h_d(\theta(\boldsymbol{q})) \tag{8}$$

where $h_s(\boldsymbol{q}) \in \mathbb{R}^N$ is also an independent joint angle function. The control objective is to force $h_s(\boldsymbol{q})$ to follow $h_d(\theta(\boldsymbol{q}))$ or, in other words, to drive the error $\boldsymbol{e}$ in (8) to zero over multiple iterations. After taking the second-order time derivative of (8), the following differential equation can be obtained:

$$\frac{d^2\boldsymbol{e}}{dt^2} = L_f^2 h(\boldsymbol{q}) + L_{\boldsymbol{g}_E} L_f h(\boldsymbol{q})\boldsymbol{u}_E + L_{\boldsymbol{g}_M} L_f h(\boldsymbol{q})\boldsymbol{u}_M \tag{9}$$

where $L_f^2 h(\boldsymbol{q})$ is the second-order Lie derivative of $h(\boldsymbol{q})$ and $L_{\boldsymbol{g}_M} L_f h$ and $L_{\boldsymbol{g}_E} L_f h$ are the decoupling matrices.

To facilitate the design of an ILC, $\bar{\boldsymbol{e}}_1^{(i)}$, $\bar{\boldsymbol{e}}_2^{(i)}$, $\boldsymbol{u}_1^{(i)}$, and $\boldsymbol{u}_2^{(i)} \in \mathbb{R}$ are defined as $\bar{\boldsymbol{e}}_1^{(i)} = \boldsymbol{e}_i$, $\bar{\boldsymbol{e}}_2^{(i)} = \dot{\boldsymbol{e}}_i$, $\boldsymbol{u}_1^{(i)} = \boldsymbol{u}_{E_i}$, and $\boldsymbol{u}_2^{(i)} = \boldsymbol{u}_{M_i}$, where i represents the ith element of the corresponding vector. Using (9), the errors because of the ILC in the kth iteration can be rewritten as

$$\begin{aligned}\dot{\bar{\boldsymbol{e}}}_{1,k}^{(i)} &= \bar{\boldsymbol{e}}_{2,k}^{(i)} \\ \dot{\bar{\boldsymbol{e}}}_{2,k}^{(i)} &= \boldsymbol{\sigma}^{T^{(i)}} \boldsymbol{v}_{f_{1,k}}^{(i)} + \boldsymbol{v}_{f_{2,k}}^{(i)} + \boldsymbol{\Omega}_k^{(i)} \boldsymbol{u}_{1,k}^{(i)} + \boldsymbol{v}_g^{(i)} \boldsymbol{u}_{2,k}^{(i)} + \boldsymbol{v}_{d,k}^{(i)}\end{aligned} \tag{10}$$

where k denotes the kth iteration, $\boldsymbol{v}_{f_{2,k}}^{(i)} + \boldsymbol{\sigma}^{T^{(i)}} \boldsymbol{v}_{f_{1,k}}^{(i)}$ is equal to the ith element of $L_f^2 h(\boldsymbol{q})$, and $\boldsymbol{v}_g^{(i)}$ and $\boldsymbol{\Omega}_k^{(i)}$ are equal to the ith element of $L_{\boldsymbol{g}_M} L_f h(\boldsymbol{q})$ and $L_{\boldsymbol{g}_E} L_f h(\boldsymbol{q})$, respectively, for the ith input. $\boldsymbol{\sigma}^{T^{(i)}} \boldsymbol{v}_{f_{1,k}}^{(i)}$ is the linearly parameterizable part of $L_f^2 h(\boldsymbol{q})$, and $\boldsymbol{v}_{f_{2,k}}^{(i)}$ is the not linearly parameterizable part of $L_f^2 h(\boldsymbol{q})$. In (10), $\boldsymbol{v}_{d,k}^{(i)}$ is the system disturbance term because of modeling uncertainty and is bounded by

$$\left|\boldsymbol{v}_{d,k}^{(i)}\right| \leq \bar{\upsilon}_d \in \mathbb{R}^+. \tag{11}$$

Without loss of generality, the superscript i ($i = 1, 2, \ldots, N$) will be dropped hereafter. $\boldsymbol{\sigma}^T$ is an unknown state-independent function, which will be learned by an iterative learning method, and $\upsilon_{f_{2,k}}$ and Ω_k will be learned by NNs. $\upsilon_{f_{2,k}}$ and Ω_k are represented by two NNs as

$$\upsilon_{f_{2,k}} = \boldsymbol{W}^T \boldsymbol{\Theta}_k(\boldsymbol{V}^T \boldsymbol{X}_k) + \varepsilon_{1,k}(\boldsymbol{X}_k) \tag{12}$$

$$\Omega_k = \boldsymbol{R}^T \boldsymbol{\phi}_k(\boldsymbol{X}_k) + \varepsilon_{2,k}(\boldsymbol{X}_k) \tag{13}$$

where $\boldsymbol{X}_k \in \mathbb{R}^{2N+1}$ is the augmented input vector for two NNs and is defined as $\boldsymbol{X}_k = \left[1\ \boldsymbol{x}_k^T\right]^T$, where $\boldsymbol{x}_k^T = \left[\boldsymbol{q_k}^T,\ \dot{\boldsymbol{q}}_{\boldsymbol{k}}^T\right]^T$. The NNs' ideal weight matrices are $\boldsymbol{W} \in \mathbb{R}^{N_2+1}$, $\boldsymbol{V} \in \mathbb{R}^{2N+1\times N_2}$, and $\boldsymbol{R} \in \mathbb{R}^{N_\Omega}$. The input layer is made of $2N+1$ neurons, N_2 and N_Ω are the number of neurons in the hidden layer of the NNs, and N is the number of output layer neurons. The NN activation function in (12) that maps the input layer to the hidden layer is denoted as $\boldsymbol{\Theta}_k : \mathbb{R}^{N_2} \to \mathbb{R}^{N_2+1}$. The activation function in (13) that maps the input layer to the output layer is denoted as $\boldsymbol{\phi}_k : \mathbb{R}^{2N+1} \to \mathbb{R}^{N_\Omega}$. The unknown functional reconstruction errors for the two NNs are denoted as $\varepsilon_{1,k} \in \mathbb{R}$ and $\varepsilon_{2,k} \in \mathbb{R}$ and are bounded as $\left|\varepsilon_{1,k}\right| \leq \bar{\varepsilon}_1$ and $\left|\varepsilon_{2,k}\right| \leq \bar{\varepsilon}_2$, where $\bar{\varepsilon}_1,\ \bar{\varepsilon}_2 \in \mathbb{R}^+$. The estimates of the ideal NNs that approximate $\upsilon_{f_{2,k}}$ and Ω_k will be learned in an iterative fashion. The kth iteration of their estimates, denoted as $\hat{\upsilon}_{f_{2,k}}$ and $\hat{\Omega}_k$, are represented as

$$\hat{\upsilon}_{f_{2,k}} = \hat{\boldsymbol{W}}_k^T \boldsymbol{\Theta}_k(\hat{\boldsymbol{V}}_k \boldsymbol{X}_k) \tag{14}$$

$$\hat{\Omega}_k = \hat{\boldsymbol{R}}_k^T \boldsymbol{\phi}_k(\boldsymbol{X}_k) \tag{15}$$

where $\hat{\boldsymbol{W}}_k \in \mathbb{R}^{N_2+1}$, $\hat{\boldsymbol{V}}_k \in \mathbb{R}^{2N+1\times N_2}$, and $\hat{\boldsymbol{R}}_k \in \mathbb{R}^{N_\Omega}$ are the estimates of ideal weights in kth iteration.

A. Top-Level Controller

Now we introduce the closed-loop controller that is commonly used by FES and the exoskeleton. The closed-loop feedback component, U_k, is defined as

$$U_k = -F_{1,k} - \hat{\upsilon}_{f_{2,k}} - \hat{\sigma}_k \upsilon_{f_{1,k}} \tag{16}$$

where $\hat{\sigma}_k$ is an estimate for σ and is computed as

$$\hat{\sigma}_k = \begin{cases} \hat{\sigma}_{k-1} - b_q \upsilon_{f_{1,k}}(\gamma s_k), & k > -1 \\ 0, & k = -1 \end{cases} \tag{17}$$

where $b_q \in \mathbb{R}^+$ is a positive constant and $s_k \in \mathbb{R}$ is a sliding surface. Note that the first iteration (here the first sit-to-stand iteration) starts from $k = 0$. In each iteration $\hat{\sigma}_k$ is obtained based on the previous iteration, hence a predefined value of $\hat{\sigma}_k$ for use in the first iteration. s_k is evaluated as

$$s_k = \lambda_1 \bar{e}_{1,k}(t) + \lambda_2 \bar{e}_{2,k}(t) \tag{18}$$

where $\lambda_i \in \mathbb{R}^+$ ($i = 1, 2$) are positive constants. In (16), $F_{1,k}$ is described as

$$F_{1,k} = \frac{1}{\lambda_2}\left(\lambda_1 \bar{e}_{2,k} + \lambda_2\left(\alpha_3 s_k + \frac{4}{3}\alpha_2 \operatorname{sgn}(s_k)\right) - \lambda_2 \upsilon_k\right) \tag{19}$$

where $\alpha_2, \alpha_3 \in \mathbb{R}^+$ and $\upsilon_k \in \mathbb{R}$ are an integral terms that are defined as

$$\dot{\upsilon}_k = -\beta_1 s_k - \beta_2 \upsilon_k \tag{20}$$

where β_1 and $\beta_2 \in \mathbb{R}^+$ are positive constants.

B. FES Controller

The controller in (16) is assigned to FES as an input u_1 at the kth iteration as

$$u_{1,k} = -\imath_n \psi_k^{-1} U_k \tag{21}$$

where $\imath_n$ is an FES allocation coefficient and ψ_k is defined as

$$\psi_k = \hat{\Omega}_k + \left(\varrho\left(\hat{\Omega}_k\right) + \beta\right) \tag{22}$$

where ψ_k is designed to avoid a singularity in ψ_k^{-1} when $\hat{\Omega}_k$ is equal to zero. The spectral radius of $\hat{\Omega}_k$, $\varrho_k\left(\hat{\Omega}_k\right) \in \mathbb{R}^+$, and a control gain, $\beta \in \mathbb{R}^+$, are added to ψ_k to avoid the singularity [41], [42].

C. Electric Motor Controller

The controller in (16) is assigned to the electric motor as an input, $u_{2,k}$, as

$$u_{2,k} = -\varsigma_n \upsilon_g^{-1} U_k \tag{23}$$

where ς_n is an allocation coefficient for the electric motors. The pair of allocation coefficients ($\imath_n$, ς_n) are introduced to deal with the input redundancy and can be switched arbitrarily as long as the following conditions are satisfied:

$$\imath_n + \varsigma_n = 1 \tag{24}$$

$$\left|u_{1,k}\right| \leq 1. \tag{25}$$

Remark: $u_{1,k}$ is a normalized stimulation variable that is mapped to an actual stimulation amplitude using a recruitment mapping [43], [44]. Because of saturation, the normalized variable may saturate and become equal to 1, but this does not affect stability because of the use of additional feedback from the electric motor in (23).

D. NN Update Laws

Based on the subsequent stability analysis, weight matrices for NNs in (14) are calculated as

$$\hat{\boldsymbol{W}}_{k_j} = \hat{\boldsymbol{W}}_{(k-1)_j} - \kappa_1 \frac{\partial E_b}{\partial \hat{\boldsymbol{W}}_{(k-1)_j}} \tag{26}$$

$$\hat{\boldsymbol{V}}_{k_j} = \hat{\boldsymbol{V}}_{(k-1)_j} - \kappa_2 \frac{\partial E_b}{\partial \hat{\boldsymbol{V}}_{(k-1)_j}} \tag{27}$$

where $\kappa_1 \in \mathbb{R}^+$ and $\kappa_2 \in \mathbb{R}^+$ are user-defined positive constants and E_b is defined as

$$E_b = \frac{1}{2}\left(\hat{v}_{f_{2,k}} - \hat{v}_{f_{2,k-1}} + \xi \gamma s_k\right)^2 \tag{28}$$

$$\hat{v}_{f_{2,k}} = 0 \text{ when } k = -1 \tag{29}$$

where $\xi \in \mathbb{R}^+$ and $\gamma \in \mathbb{R}^+$ are positive constants. Note that the first iteration (here the first sit-to-stand iteration) starts from $k = 0$. In each iteration, $\hat{v}_{f_{2,k}}$ is obtained based on the previous iteration. Accordingly, a predefined value of $\hat{v}_{f_{2,k}}$ when $k = -1$ is used in the first iteration. Additionally, based on subsequent stability analysis, the following update law is designed for $\hat{\boldsymbol{R}}_k$ in (15):

$$\dot{\hat{\boldsymbol{R}}}_k = \phi_k(\boldsymbol{X}_k) u_{1,k} s_k. \tag{30}$$

E. Stability Analysis and Finite Time Convergence

Theorem 1: The control inputs in (21) and (23) ensure asymptotic stability of the subsystems in (10) ($\forall$ i=1, . . . , N), i.e., $\bar{e}_1^{(i)}$ *approaches zero with time* despite arbitrary switching of allocation coefficients (ι_n, ς_n) that are constrained as in (24), provided that the control gains are chosen as $\beta_2 > 2$ and $\alpha_3 > 2/\lambda_2$, where β_2 and α_3 are defined in (19) and (20).

The details of stability analysis for our novel control algorithm are provided in the Appendix.

V. Experimental Procedure and Results

The experimental study was approved by the Institutional Review Board (IRB) at the University of Pittsburgh (IRB approval number: PRO 14040419) and North Carolina State University (IRB approval number: 20533). All participants signed an informed consent form before participating in the experiments. Four participants without any neuromuscular disorders were involved in this study (Age 24.3±0.9, all male). One participant with complete SCI was also involved in this study (Age 51, male, injury level: T11).

In Fig. 2, the experimental setup and control algorithm are illustrated. The testbed consists of two DC brushless servo motors (Harmonic Drive Company, USA), which have a maximum speed of 30 revolutions per minute (RPM) for both hips, two 90-watt DC motors (Maxon Motor Inc., Switzerland) for both knees, and two sets of FES electrode pads for the quadriceps muscles. The gearbox ratio for both knee and hip joints is 100:1. Two incremental optical encoders with 4000 pulses per revolution (PPR) resolution were used to measure hip joint angles, and two inductive encoders with 4096 PPR resolution were used to measure knee joint angles. In this experimental setup, the exoskeleton joint motors are not

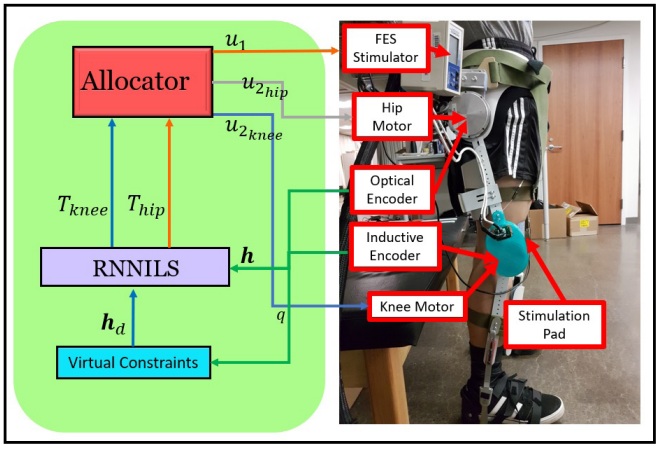

Fig. 2. Hybrid exoskeleton testbed used for the experiments and the diagram of the control algorithm.

backdrivable. Our goal was not to use FES solely. Therefore, using backdrivable motors was not essential. Additionally, the quadriceps muscle group is the single directional agonist muscle group, and it was used for single directional knee extension work for a sit-to-stand task. Therefore, during cooperative control, the FES-based muscle forces and knee joint motors will not be against each other.

A biphasic stimulation train was applied to the surface electrodes using a RehaStim 8-channel stimulator (Hasomed Inc., DE), where the pulse trains had a frequency of 35 Hz and the stimulation pulsewidth was chosen as 400 μs. For ensuring patient safety, several precautions were taken, including an emergency stop button held by a researcher to cut power to the device, and another emergency button on the walker, which was accessible to the participant. Several safety measures incorporated in the motor controller limit the maximum joint angles to prevent hip hyperextension and knee hyperextension. The controller was programmed in Simulink (MathWorks Inc., USA) and implemented using a real-time target machine (Speedgoat Inc., Liebefeld Switzerland) with a frequency of 350 Hz, which modulated the stimulation current amplitude and the current amplitudes of the exoskeleton motors during the experiments. Both the thigh and shank frames of the exoskeleton are designed to be length adjustable to meet the requirements of different participants. The width of the stabilization belt on the waist can also be adjusted to fit the participants.

The participants were instructed to relax and avoid any voluntary interference with the exoskeleton through the entire experimental procedure. Also, to further minimize the voluntary interference with the hybrid exoskeleton control, the participants were not allowed to view the control performance or the desired virtual constraints on the computer screen. Four sets of experiments on each participant were conducted to evaluate the newly proposed ILC. Each experimental set included four iterations. Each iteration of the sit-to-stand procedure was run for 20 s. This time duration was designed as per the participant's convenience to use the exoskeleton. The desired movement profile allows a participant to achieve a sit-to-stand in about 5–7.5 s. The remaining time is

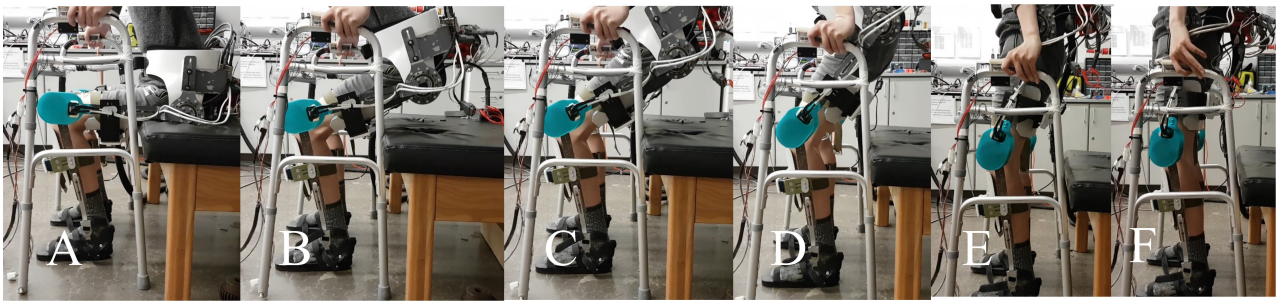

Fig. 3. Snapshots of the standing up experiment performed on Participant 1.

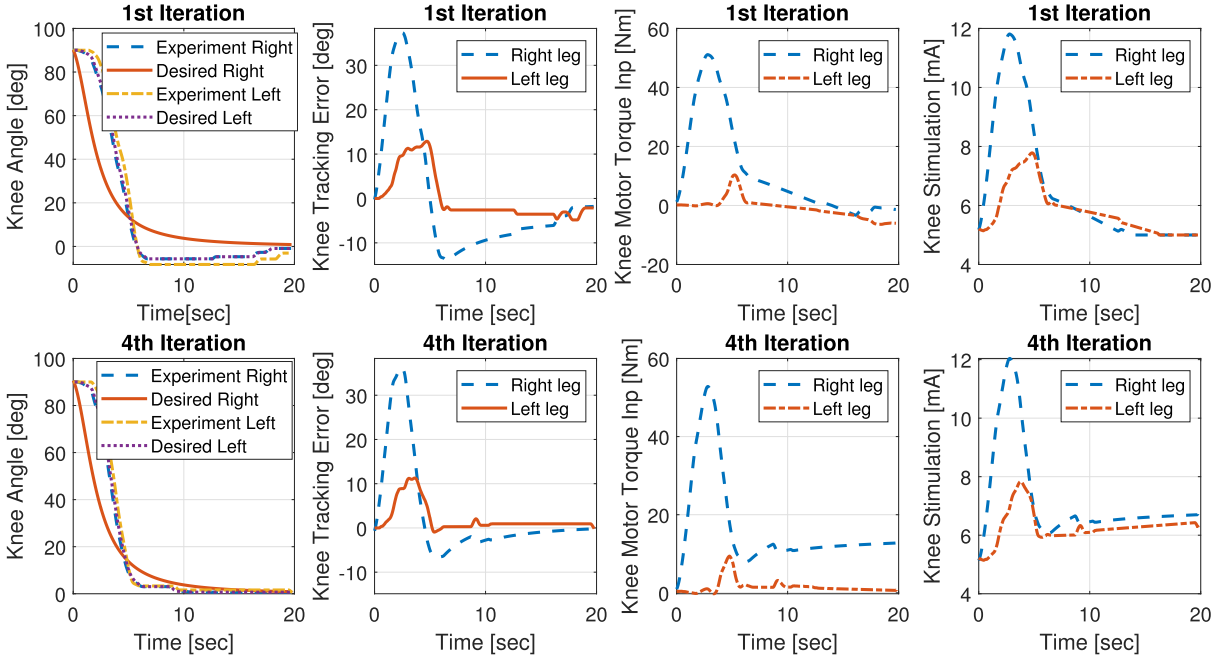

Fig. 4. Knee joints angular profiles, tracking errors, and control inputs of Participant 1 for the 1st iteration and the 4th iteration, where $\iota_n = 0.2$ and $\varsigma_n = 0.8$.

allocated to check control performance in the standing mode. Between two successive iterations, the participants rested for one minute. The resting period was provided to allow the muscles to recover in case of FES-induced fatigue. Fig. 3 depicts snapshots of the sit-to-stand movement on Participant 1 while wearing the hybrid exoskeleton.

In initial experiments, allocation coefficients of $\iota_n = 0.2$ and $\varsigma_n = 0.8$ were chosen. In Fig. 4, knee angle profiles, knee angle tracking errors, and knee control inputs are shown for Participant 1 for the 1st and 4th iterations. In Fig. 5, hip angle profiles, hip angle tracking errors, and hip control inputs are shown for Participant 1 for the 1st and 4th iterations. According to these two figures, in the 4th iteration, the system can track the desired movement profile more accurately. Despite a high model uncertainty, i.e., because of differences between the dynamic model and the real system, and having different participants in the device, the controller could still limit the error and provide a smooth sit-to-stand movement for the participant after only four iterations.

The resulting knee and hip control inputs of the motors and FES of the hybrid exoskeleton are shown in Figs. 4 and 5, respectively. The knee stimulation profiles shown here are mapped from the normalized stimulation variable using a recruitment mapping [44].

The control framework was also validated on a participant with SCI. The results in Fig. 6 show the proposed framework could work successfully for the participant with SCI. Fig. 6 shows the snapshots that illustrate the movement produced during the experiments for Participant 5 (the subject with complete SCI).

The results in Figs. 7 and 8 illustrate knee joint performance and control inputs and hip joint performance and control inputs, respectively, in the 1st and 4th iterations for Participant 5. As shown in the figures, the controller could successfully force the system to track the desired movement profile. The controller used a higher gain to let Participant 5 experience an easier sit-to-stand movement. Furthermore, a different movement profile was used for Participant 5 to account for his hip joint limitations. These joints' angular limitations are because of his SCI and the long-term use of a wheelchair.

The results in Figs. 4 and 7 show the input torques and the trajectory tracking errors of the right knee are higher than

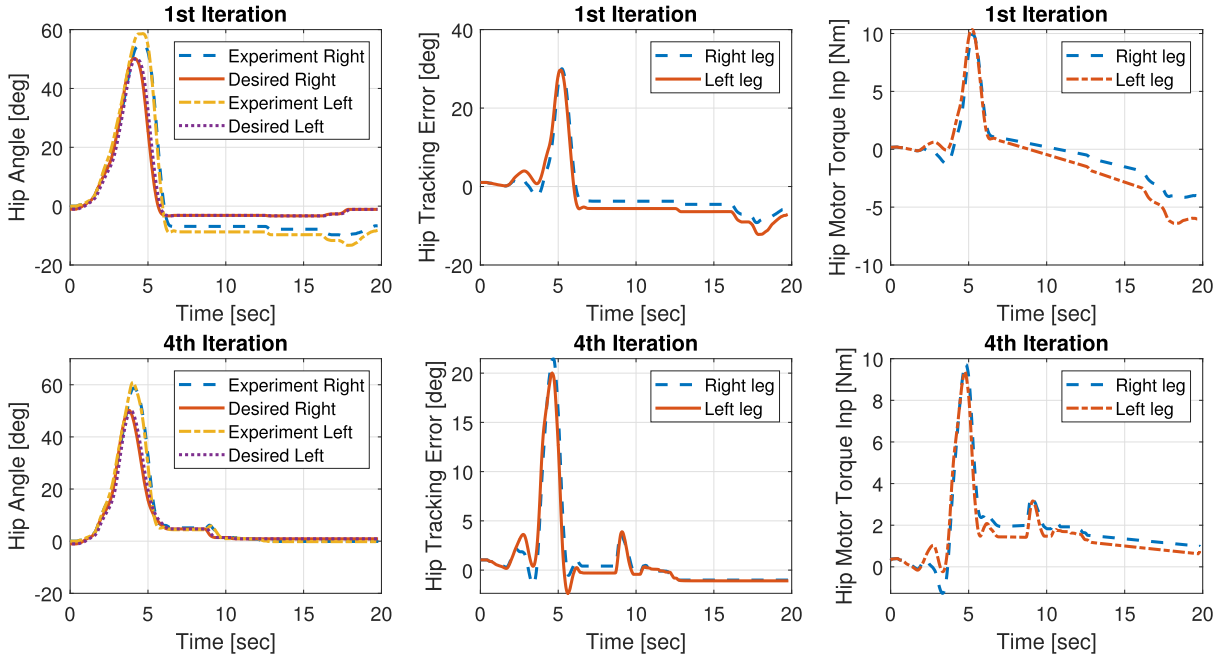

Fig. 5. Hip joints angular profiles, tracking errors, and control inputs of Participant 1 for the 1st iteration and the 4th iteration, where $\iota_n = 0.2$ and $\varsigma_n = 0.8$.

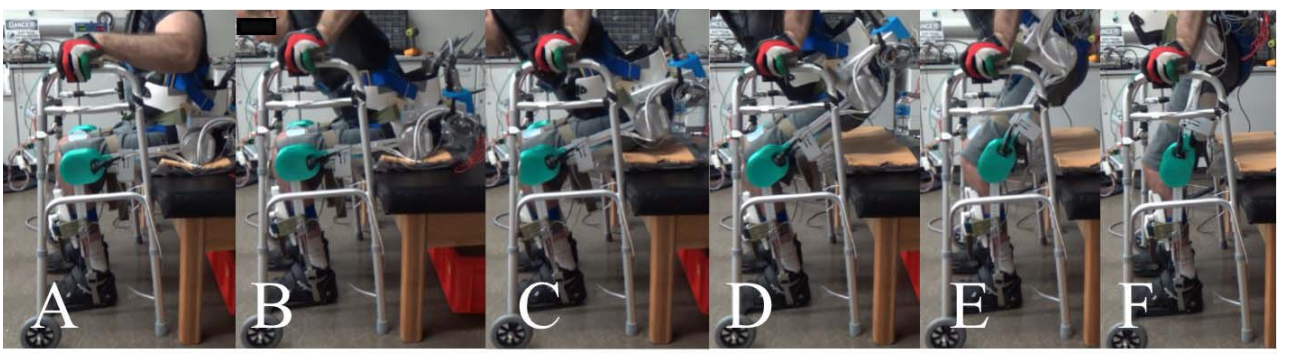

Fig. 6. Snapshot sequences of Participant 5 with complete SCI for a sit-to-stand scenario.

those of the left knee. This is because the virtual constraints, used as the desired profiles for the joints, take the right joint angular position as the base, and the other joints' desired profiles are derived based on the right joint's actual angular position. Therefore, the right knee joint leads the left knee joint during the movement and at the initiation of the task. Because the right knee joint is the joint that initiates the task, it needs higher torque, and the tracking is more challenging for this joint.

The control input for SCI participant, shown in Fig. 7, is more oscillatory in comparison to the control input of the able-bodied participant in Fig. 5, because higher control gains were used for the SCI participant. The results in Figs. 7 and 8 show that the final knee and hip joint positions are greater than zero. The reason is that different desired profiles are applied for Participant 5 because his knee and hip joints cannot be extended to the straight position due to joint contractures. Therefore, to support the participant's final standing posture, the knee and hip joints' motors and FES are required to generate nonzero inputs even toward the end of the experiment. Fig. 9 provides a representative result (Participant 5) to depict how the estimates of the linearly parameterizable part, $\hat{\sigma}\upsilon_{f_1}$, and the estimates of the not linearly parameterizable part, $\hat{\upsilon}_{f_2}$, of the system model adapt over multiple iterations.

Root mean square error (RMSE) between each joint's desired and actual joint trajectories was calculated during each sit-to-stand trial. Under the allocation coefficients of $\iota_n = 0.1$ and $\varsigma_n = 0.9$, the mean RMSE values in each iteration on both knee and hip joints from each participant are summarized in Table I. In addition, the last rows of the upper and lower halves in Table I provide the RMSE improvement percentage between the 1st and 4th iterations. According to this table, overall, after four iterations, RMSE mean values of the knee and hip joints were improved by 46.20% and 53.34%, respectively. Fig. 10 further shows the RMSE percentage of each iteration over the 1st iteration on both knee and hip joints from each participant. According to

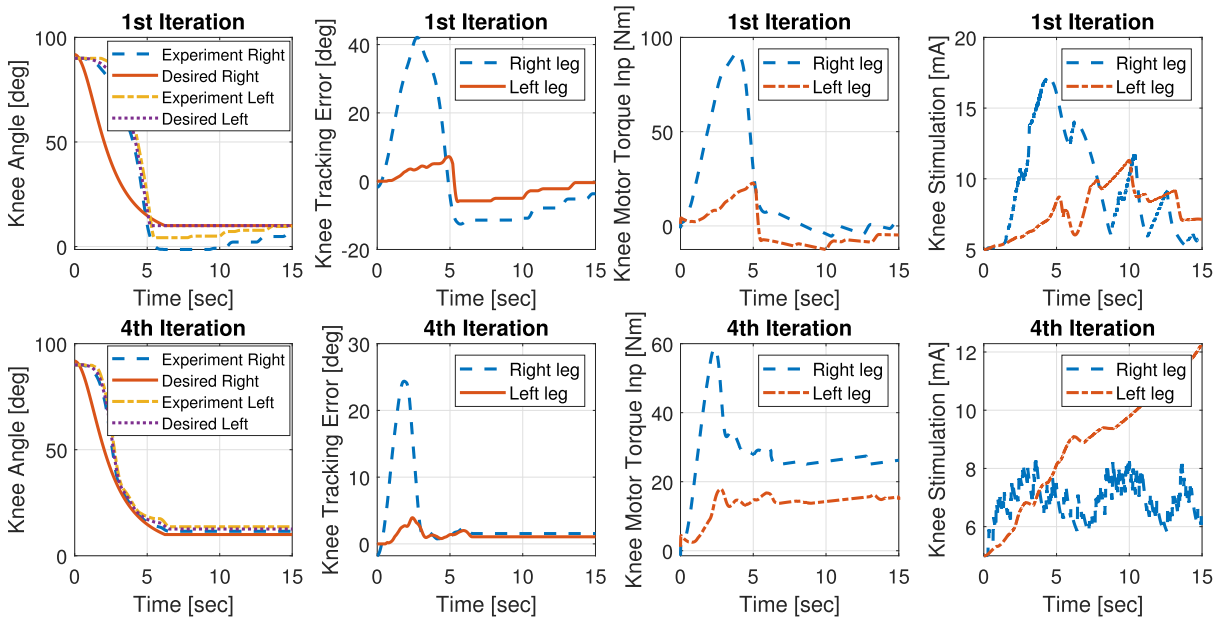

Fig. 7. Knee joints angular profiles, tracking errors, and control inputs of Participant 5 in the 1st and 4th iteration.

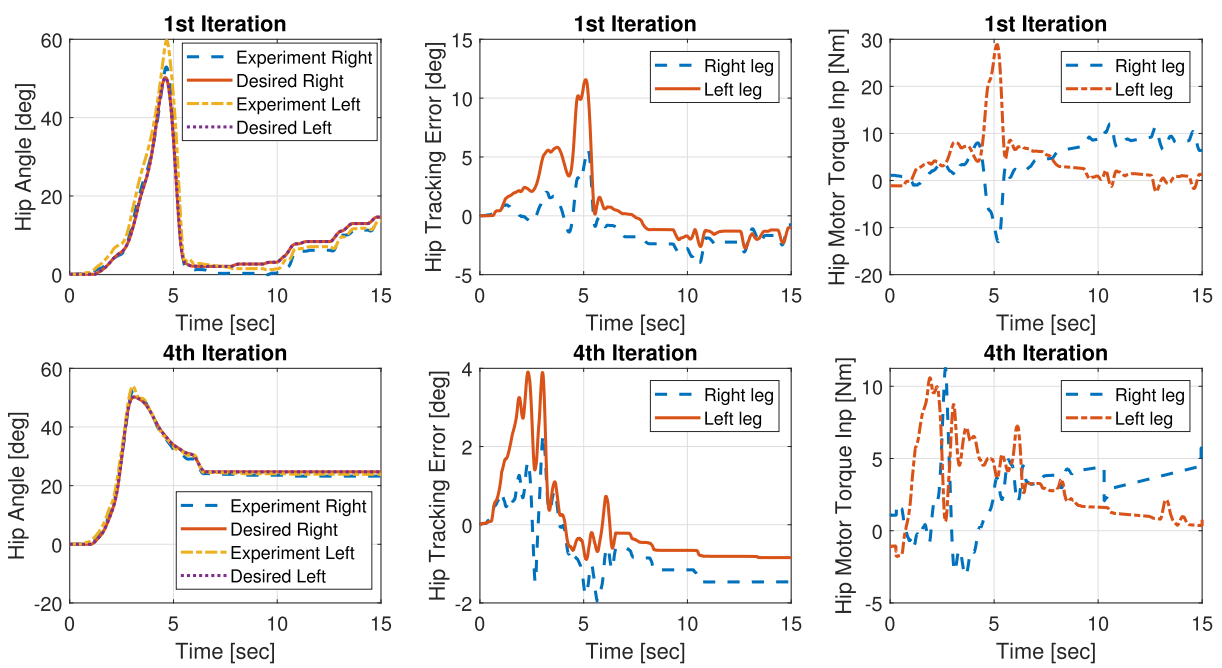

Fig. 8. Hip joints angular profiles, tracking errors, and control inputs of Participant 5 in the 1st and 4th iteration.

this figure, for Participant 1, RMSE of the right knee, left knee, right hip, and left hip were improved by 53%, 59%, 59%, and 62%, respectively. Similarly, for Participant 2, RMSE of the right knee, left knee, right hip, and left hip were improved by 43%, 46%, 60%, and 61%, respectively. Furthermore, for Participant 3, a similar trend of improvement can be seen such that RMSE of the right knee, left knee, right hip, and left hip were improved by 40%, 46%, 53%, and 50%, respectively. Finally, for Participant 5 (SCI participant), RMSE of the right knee, left knee, right hip, and left hip were improved by 63%, 44%, 41%, and 63%, respectively.

To determine the robustness of the developed control method to the switching allocation between FES and exoskeleton motors, the allocation ratio was switched twice during the experiments. We changed the exoskeleton motors and FES allocation ratio from $\varsigma_n = 0.7$, $\iota_n = 0.3$ in the first set of iterations to $\varsigma_n = 0.8$, $\iota_n = 0.2$ in the second set of iterations and $\varsigma_n = 0.9$, $\iota_n = 0.1$ in the final set of iterations. The results of this switching on Participant 1 can be seen in Fig. 11. In this figure, RMSE of joint angular positions for different iterations and for the two switching scenarios are shown. It can be observed that after switching, the system remains stable,

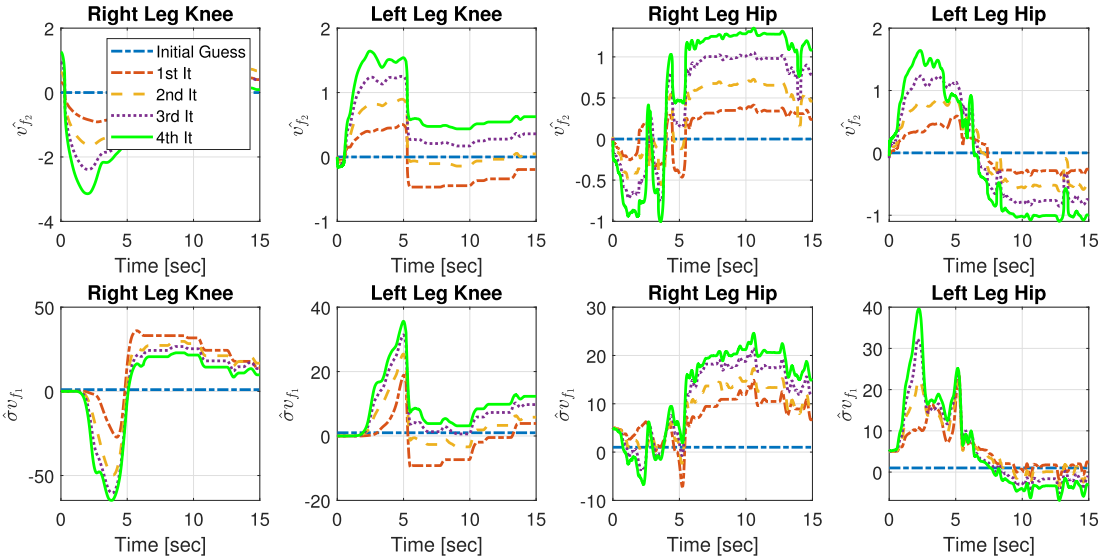

Fig. 9. Linearly parameterizable part estimation, $\hat{\sigma} v_{f_1}$, and the not linearly parameterizable part estimation, $\hat{v}_{f_2}$, of the system dynamics for Participant 5 with complete SCI.

TABLE I

RMSE MEAN VALUES OF JOINT ANGULAR POSITION TRACKING RESULTS ON EACH PARTICIPANT IN DIFFERENT ITERATIONS WHERE $\iota_n = 0.1$ AND $\varsigma_n = 0.9$ (RK: RIGHT KNEE, LK: LEFT KNEE, RH: RIGHT HIP, LH: LEFT HIP)

RMSE [deg]	Participant 1				Participant 2				Participant 3			
	RK	LK	RH	LH	RK	LK	RH	LH	RK	LK	RH	LH
1st iteration	10.09	14.35	13.01	14.87	6.72	8.81	11.93	11.43	9.88	12.31	15.82	15.01
2nd iteration	7.90	9.57	9.14	10.36	4.87	5.59	7.74	6.35	7.61	8.39	10.98	9.72
3rd iteration	7.29	8.99	8.85	9.00	3.91	4.75	5.99	5.43	6.64	7.21	8.19	7.56
4th iteration	4.71	5.88	5.24	5.59	3.78	4.70	4.74	4.37	5.90	6.59	7.43	7.39
Improvement [%]	53.32	59.02	59.72	62.41	43.75	46.65	60.27	61.77	40.28	46.47	53.03	50.77

RMSE [deg]	Participant 4				Participant 5			
	RK	LK	RH	LH	RK	LK	RH	LH
1st iteration	1.53	0.99	1.70	2.89	11.84	3.43	1.70	3.13
2nd iteration	1.17	0.73	1.49	2.02	9.07	3.16	1.49	2.16
3rd iteration	1.13	0.69	1.43	1.59	5.01	2.21	1.46	1.22
4th iteration	1.08	0.64	1.16	1.50	4.33	1.91	1.20	1.13
Improvement [%]	29.41	35.35	31.76	48.09	63.43	44.31	41.67	63.90

and the RMSE continues decreasing under the same allocation ratio. Although the trajectory tracking errors increase initially, the system starts to learn and reduces the error again.

A. Comparison with Existing Controllers

Another issue that may arise when deploying a new control method is the question about the benefits of the new method over the previous method(s). We mentioned the benefits of the novel NNILC in the introduction section. To show its benefits, the NNILC was compared experimentally with a PD control method and an ILC method developed in [45]. This ILC method was implemented as

$$U_k = -F_{2,k} - \hat{\sigma}_k v_{f_{1,k}}$$

where $F_{2,k}$ is a feedback part. The PD control method was implemented as

$$U_k = C_1(\lambda_1 \bar{e}_{1,k} + \lambda_2 \bar{e}_{2,k})$$

where C_1 is a constant gain. The other terms of both the PD and the ILC methods were introduced in the previous sections. More details of the implementation and stability analysis of the previously developed ILC method is presented in [45]. Figs. 12 and 13 show the experimental results obtained from implementing the PD, the ILC, and the novel NNILC method developed in this article. Fig. 12 shows each method's RMSE improvements over four iterations. The results in this figure are the mean over six trials. The PD control method resulted in RMSE improvement less than 10% across all iterations, which was expected due to its noniterative nature. On the contrary, the ILC method could improve the right knee, left knee, right hip, and left hip RMSEs by 18.93%, 6.35%, 17.50%, and 20.36%, respectively. The novel NNILC could also improve the right knee, left knee, right hip, and left hip RMSEs by 32.15%, 39.98%, 30.08%, and 42.71%, respectively, which are 1.70, 6.29, 1.72, and 2.10 times higher than the sole ILC method, respectively.

We focused on the fourth iteration's RMSE reduction percentage by using the three controllers for statistical analysis. For each group, there were six RMSE reduction percentage values (six sit-to-stand trials) obtained from the same participant. A Shapiro–Wilk test was used to determine the normality

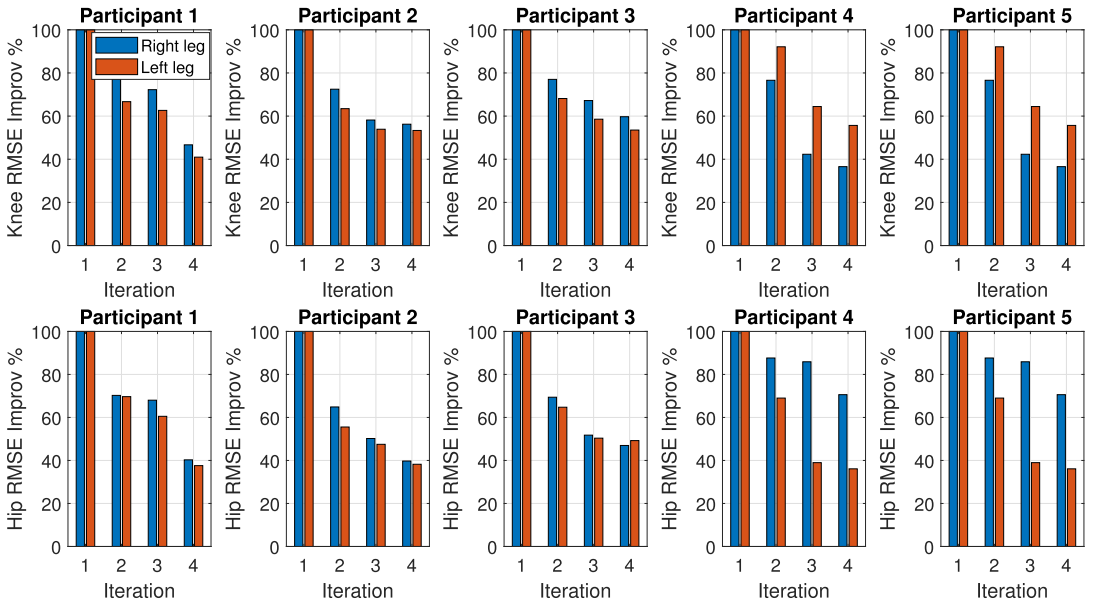

Fig. 10. Means of RMSE improvement percentage on both knee and hip joints in different iterations across all participants, where $\iota_n = 0.1$ and $\varsigma_n = 0.9$.

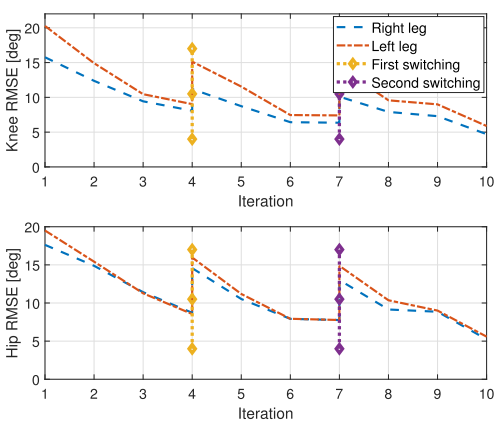

Fig. 11. RMSE values of angular position tracking from two allocation ratio impulse switches on Participant 1.

of the data. The results did not show a normal distribution of the data. Therefore, a Kruskal–Wallis test was used to determine whether there was a significant difference among the three groups' percentage values for each joint. When a significant difference was identified ($p < 0.05$), post-hoc Tukey's honestly significant difference tests were applied to determine the significant difference between the reduction percentages obtained using NNILC and ILC or NNILC and PD controllers. The results show that for the right knee joint, the RMSE reduction performance is significantly better by using NNILC than by using ILC ($p = 0.046$) and PD ($p = 0.034$) controllers. For the left knee joint, the RMSE reduction performance is significantly better by using NNILC than by using ILC ($p = 0.014$) and PD ($p = 0.012$) controllers. For the right hip joint, the RMSE reduction performance is significantly better by using NNILC than by using ILC ($p = 0.038$) and PD ($p = 0.022$) controllers. For the left hip joint, the RMSE reduction performance is significantly better by using NNILC than by using ILC ($p = 0.048$) and PD ($p = 0.002$) controllers.

The joint trajectory tracking results obtained by implementing these three controllers in the 4th iteration sit-to-stand trial on Participant 4 are shown in Fig. 13, where the first row demonstrates joint angular position change of both desired and actual trajectories, and the second row displays the corresponding tracking errors of each joint on this participant. This figure shows that the proposed novel NNILC method could achieve better trajectory tracking performance during the sit-to-stand experiments compared to traditional ILC and PD controller methods.

VI. Discussion

A hybrid exoskeleton that uses a combination of FES and a powered exoskeleton can potentially enable people with paraplegia to stand and walk again. We were motivated to design a controller that can iteratively learn a participant's musculoskeletal model, thus potentially easing its implementation in clinics with minimal tuning. Furthermore, we were interested in guaranteeing that task stability and performance are not compromised when FES and exoskeleton motor allocation levels are switched or changed by a clinician or physical therapist. To achieve these objectives, a robust NN-based ILC was derived and validated through sit-to-stand experiments. Compared to FES-induced standing, such as the systematic approach mentioned in [46], the knee motor on the powered exoskeleton could share the workload of the knee extension effort during the standing up procedure, which could also improve knee extensors' fatigue resistance. Because of day-to-day and interperson variations in the musculoskeletal models and the tedious process needed to identify the model [20], [47], it is challenging to implement existing controllers for hybrid exoskeletons in clinics. Although numerous articles on FES control exist that use high-gain controllers [48], [49] to provide robustness to modeling uncertainties or even adapt and learn the model using neural networks [36], [50]–[52], their implementation may need extensive tuning or offline training

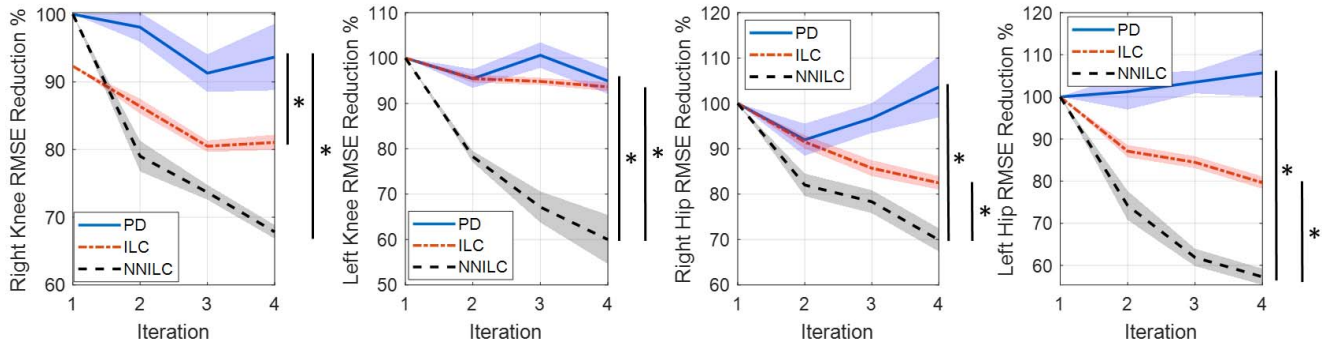

Fig. 12. Comparison of the improvements in the mean RMSE because of the novel NNILC method and the ILC method for Participant 4. The center line represents the mean over six trials, and the shaded region is one standard deviation. The asterisks represent statistical significance level ($p < 0.05$).

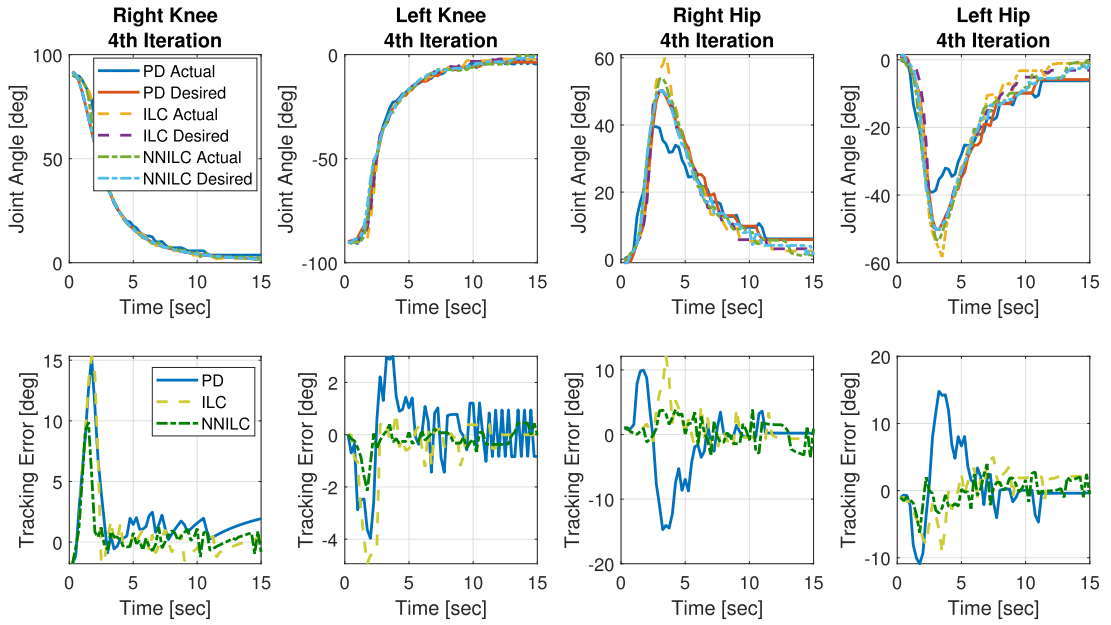

Fig. 13. Knee and hip joints angular position and tracking error results of Participant 4 in the 4th iteration. The rotation direction signs for the left and right joints are defined to be opposite to each other.

of NNs. These procedures make the job of a clinician or physical therapist difficult because they may not have control engineering experience. This problem arises when there are several parameters that they can tune but the parameters may have coupled performance effects. The control method proposed in this article addressed these problems by tuning some of the parameters through an ILC method. ILC is a class of controllers that learn modeling uncertainties while improving control performance in consecutive iterations or task cycles. This ILC method was used to control a solely FES system for upper limb stroke rehabilitation in [53]. The method was also recently depicted for ankle exoskeleton control in [54] and for knee orthosis control in [34]. Unlike these methods, the proposed approach uses NNs for learning system dynamics and using allocation coefficients to coordinate FES and the electric motors in the hybrid exoskeleton. The experimental results clearly show that the NN-based ILC method performs better than the traditional ILC method. These results were found to be statistically significant. Furthermore, using a real-time NN estimation as a feedforward component can help the system adapt and potentially avoid using a high-gain feedback controller, e.g., a PD controller. The experimental results clearly show that the controller consistently reduces RMSEs in every iteration, unlike the PD controller. These results were found to be statistically significant.

A switching strategy has recently been used in hybrid systems such as a hybrid system with FES and a motorized bike [55]–[57]. In these switched control design methods, the joint angle state determines stimulation and control timings of different muscle groups and the motor-driven cycle. Unlike these switching control approaches, the control technique in this article is designed for a sit-to-stand task, where FES and the electric motor use predetermined allocation levels that can be switched appropriately with the onset of muscle fatigue. As shown in the experimental results, the control framework can potentially allow a user or a physical therapist to change the torque allocation between the electric motors and FES on the fly. The results show that the controller can recover

system performance when the allocation is suddenly switched. Although we showed arbitrary switching of the allocation coefficient, fatigue-based switching was not shown. We believe that this control design can be easily extended to our previous work on NMPC-based control and synergy-based control of hybrid exoskeletons [20], [27]. A fatigue-based switching strategy can be used to switch between desired synergies or change allocation levels in NMPC-based single joint control.

This work is different from [25], [31], which used virtual constraints through a partial hybrid zero dynamics technique for an exoskeleton. Our control method does not use a feedback linearization control method, unlike the authors in [25], [31], who utilized input-output linearization. Contrary to their approach, the proposed method is able to learn the uncertain time-varying dynamics in real time and thus is robust to uncertain system dynamics. Moreover, unlike the control systems in [25] and [31] that focused on a hands-free powered exoskeleton, the control method in this work has been implemented on a hybrid exoskeleton. The proposed method addresses the switched allocation problem, which is unique to hybrid exoskeleton control. However, their use of virtual constraints in their control design inspired us to design virtual constraint-like desired trajectories that can be beneficial for multijoint wearable hybrid exoskeletons. Time-dependent trajectories, which may be designed independently for each lower limb joint, may cause joint misalignment in the left and right legs if there is a miscoordination during trajectory tracking. This situation can be potentially unsafe and cause undesired control performance. Unlike time-dependent trajectories, virtual constraints coordinate desired joint angles through a single monotonically increasing function, potentially avoiding joint miscoordination.

Limitations: The exoskeleton setup used for this study is not backdrivable. In the experiments, our goal for using FES was supplementing the motors during sit-to-stand motions so that smaller motors can be used in the future. The current setup does not allow the use of FES alone. For example, in the case where the allocation coefficient is set as 1 for FES and 0 for motors, the exoskeleton has to be run in an admittance/impedance mode. Although we did not test this case, the results can be easily extended if an admittance or impedance control is chosen along with the proposed framework. Results shown in Figs. 4, 5, 7, and 8 indicate the time duration for the sit-to-stand task lasts around 5–7.5 s among different participants. Compared to a normal sit-to-stand task by a person with no disability, 5–7.5 s for a sit-to-stand may seem relatively long but are practical. The participant with SCI felt more comfortable, safe, and less nervous when we executed the sit-to-stand movement slowly. Unlike person with no disabilities who effortlessly coordinate their lower body joints, including the ankle and knee joints, with their upper body, sit-to-stand is challenging for a person with spinal cord injury. Usually, in this case only the knee joint powers sit-to-stand. Furthermore, with no help from the ankle joint and a lack of coordination with the upper body, the desired acceleration needed to stand up normally is limited. Also, our reported sit-to-stand times for persons with SCI are not completely unheard of in this field. Other researchers have also used slow sit-to-stand movements, e.g., please see work in [58] and [59]. Besides, the sit-to-stand times for older population or people in gait therapy, using a commercial lift system, are similar to the sit-to-stand times implemented in our article.

In future, these reference trajectories can be modified to allow faster sit-to-stand movements. The reference trajectories are designed such that the right knee follows a predesigned desired time-dependent trajectory, whereas the other joint angles follow the virtual constraints comprising the actual right knee angle as the phase variable. Therefore, the right knee joint leads the left knee joint in the movement and causes asymmetric error performances (Figs. 4 and 7) in the left and right knees. Because the right knee joint is the joint that initiates the task, it needs higher torque, and the tracking is more challenging for this joint. In this article, we focused on the sit-to-stand task because it is a precursor to walking and stand-to-sit and likely needs larger torques due to anti-gravity motion, making it equally challenging when compared to stand-to-sit and walking. However, we feel stand-to-sit may need a slightly different approach in the virtual constraint design as the goal is to bring the user smoothly downward and touch the seat almost at a zero velocity. Furthermore, sit-to-stand experiments were done as a proof-of-concept of the novel control method. In the literature, a sit-to-stand task has been frequently used in various articles for checking capability and performance of control methods [26], [60], [61]. In future studies, stand-to-sit movement will also be addressed.

Our preliminary work with one participant with SCI in this study shows that regulating the final knee and hip joints' position for a participant with SCI to zero would be challenging. Unlike participants without any neurological disabilities, different desired profiles may be needed for participants with SCI as their joints may not fully extend because of joint contractures and long-term disuse. Also, the controller gains may need to be set at higher levels because of larger disturbances while testing with participants with SCI. These disturbances could be because of spasticity, increased nervousness, or hesitation of the participant during verticalization.

VII. Conclusion

This article derives a robust and adaptive ILC framework for a hybrid exoskeleton. The control framework also allows arbitrary switching between different FES and electric motor allocation levels, as demanded by a user or a therapist. A discrete energy-based stability analysis proves asymptotic tracking of desired movement profiles and robustness to arbitrarily switched FES and exoskeleton motor allocation levels. Sit-to-stand experiments were performed on five human participants, including a person with complete paraplegia. The experimental results showed reduced angular position RMSEs of both knee and hip joints in each iteration, which validated the controller's effectiveness and robustness. The results also showed that the hybrid exoskeleton system tracked sit-to-stand movement profiles despite the switched allocation ratio between FES and the powered exoskeleton. The results show that the proposed controller can control a hybrid

exoskeleton without extensive tuning of control parameters. Future work focuses on validating the control method on more participants with SCI and designing a strategy for optimal allocation ratio switching between FES and the exoskeleton for a more general experimental scenario like walking.

Appendix

A. Stability Analysis and Finite Time Convergence

This section provides a proof for Theorem 1 and elaborates on the stability analysis of the new control method.

We call the overall robust control strategy NNILC due to the use of NN, iterative learning, and arbitrary allocation switching between feedback components of FES and the electric motor. Below, a closed-loop error system is developed for subsequent stability analysis. Using (16), (19), (21), (23), (24), and adding and subtracting $\psi_k u_{1,k}$ to (10) results in

$$\begin{aligned}\dot{\bar{e}}_{2,k} &= E_{s,k} + \Psi_k \upsilon_{f_{1,k}} + \widetilde{\Omega}_k u_{1,k} - \alpha_3 s_k \\ &\quad -\frac{4}{3}\alpha_2 \mathrm{sgn}(s_k) + \upsilon_k - \frac{\lambda_1}{\lambda_2}\bar{e}_{2,k} + \upsilon_{d,k} \end{aligned} \tag{31}$$

where $E_{s,k} = \upsilon_{f_{2,k}} - \hat{\upsilon}_{f_{2,k}}$ is the not linearly parameterizable estimation error for the NN. Additionally, $\widetilde{\Omega}_k = \Omega_k - \psi_k$ and $\Psi_k = \sigma - \hat{\sigma}_k$. Based on (13) and (22), $\widetilde{\Omega}_k$ can be expressed as

$$\widetilde{\Omega}_k = \widetilde{\boldsymbol{R}}_k^T \phi(\boldsymbol{X}_k) + \beta_{\varepsilon,k} \tag{32}$$

where $\widetilde{\boldsymbol{R}}_k = \boldsymbol{R}_k - \hat{\boldsymbol{R}}_k$, $\beta_{\varepsilon,k} = \varepsilon_{2,k} - \left(\varrho_k\left(\hat{\Omega}_k\right) + \beta\right)$, and $\beta_{\varepsilon,k}$ is bounded by

$$\left|\beta_{\varepsilon,k}\right| \le \bar{\beta}_\varepsilon \in \mathbb{R}^+. \tag{33}$$

Therefore, (31) can be written as

$$\begin{aligned}\dot{\bar{e}}_{2,k} &= E_{s,k} + \Psi_k \upsilon_{f_{1,k}} + (\widetilde{\boldsymbol{R}}_k^T \phi(\boldsymbol{X}_k) + \beta_{\varepsilon,k}) u_{1,k} \\ &\quad -\alpha_3 s_k - \frac{4}{3}\alpha_2 \mathrm{sgn}(s_k) + \upsilon_k - \frac{\lambda_1}{\lambda_2}\bar{e}_{2,k} + \upsilon_{d,k}. \end{aligned} \tag{34}$$

By taking the time derivative of s_k, the $\dot{s}_k$ dynamics is given as

$$\begin{aligned}\dot{s}_k &= \lambda_2\Big(-\alpha_3 s_k - \frac{4}{3}\alpha_2 \mathrm{sgn}(s_k) + \upsilon_k + \upsilon_{d,k} \\ &\quad + \Psi_k \upsilon_{f_{1,k}} + \beta_\varepsilon u_{1,k} + \widetilde{\boldsymbol{R}}_k^T \phi_k(X_k) u_{1,k} + E_{s,k}\Big). \end{aligned} \tag{35}$$

Let $V_k(x,t) : \mathbb{R}^N \times \mathbb{R} \to \mathbb{R}$ be an energy function where $t \in [t_0, t]$, t_0 is the start time of an iteration, and t is the elapsed time after the start of an iteration. V_k is defined as

$$V_k = V_k^{(1)} + V_k^{(2)} + V_k^{(3)} + V_k^{(4)} + V_k^{(5)} \tag{36}$$

where $V_k^{(1)} = \upsilon_k^2/2$, $V_k^{(2)} = (\gamma/\lambda_2)(s_k^2/2)$, $V_k^{(3)} = 1/2b_q \int_{t_0}^t \Psi_k^2 d\tau$, $V_k^{(4)} = 1/2\xi \int_{t_0}^t E_{s,k}{}^2 d\tau$, and $V_k^{(5)} = 1/2tr\left\{\tilde{\boldsymbol{R}}_k^T \tilde{\boldsymbol{R}}_k\right\}$. γ, b_q, $\xi \in \mathbb{R}^+$ are constants where b_q and ξ are chosen by the user and γ is subsequently defined. The difference between the first energy function in two successive iterations is computed as

$$\Delta V_k^{(1)} = V_k^{(1)} - V_{k-1}^{(1)}. \tag{37}$$

Therefore, the following expression is obtained as

$$\begin{aligned}\Delta V_k^{(1)} &= \frac{\upsilon_k^2}{2} - \frac{\upsilon_{k-1}^2}{2} \\ &= \int_{t_0}^t \upsilon_k \dot{\upsilon}_k d\tau + \frac{\upsilon_k^2(t_0)}{2} - \frac{\upsilon_{k-1}^2}{2}. \end{aligned} \tag{38}$$

By substituting (20) in equation (38), the following equation is derived as

$$\begin{aligned}\Delta V_k^{(1)} &= -\beta_1 \int_{t_0}^t \upsilon_k s_k d\tau - \beta_2 \int_{t_0}^t \upsilon_k^2 d\tau \\ &\quad + \frac{\upsilon_k^2(t_0)}{2} - \frac{\upsilon_{k-1}^2}{2}. \end{aligned} \tag{39}$$

The difference in successive iterations for the second energy function is obtained as

$$\begin{aligned}\Delta V_k^{(2)} &= \frac{\gamma}{\lambda_2}\frac{s_k^2}{2} - \frac{\gamma}{\lambda_2}\frac{s_{k-1}^2}{2} \\ &= \frac{\gamma}{\lambda_2}\int_{t_0}^t s_k \dot{s}_k d\tau - \frac{\gamma}{\lambda_2}\frac{s_{k-1}^2}{2} + \frac{\gamma}{\lambda_2}\frac{s_k^2(t_0)}{2}. \end{aligned} \tag{40}$$

By substituting (35) into (40), we have

$$\begin{aligned}\Delta V_k^{(2)} &= -\frac{\gamma}{\lambda_2}\frac{s_{k-1}^2}{2} - \gamma\alpha_3 \int_{t_0}^t s_k^2 d\tau + \frac{\gamma}{\lambda_2}\frac{s_k^2(t_0)}{2} \\ &\quad + \gamma \int_{t_0}^t s_k \Psi_k \upsilon_{f_{1,k}} d\tau - \frac{4}{3}\alpha_2 \gamma \int_{t_0}^t s_k \mathrm{sgn}(s_k) d\tau \\ &\quad + \gamma \int_{t_0}^t s_k \upsilon_{d,k} d\tau + \gamma \int_{t_0}^t s_k \widetilde{\boldsymbol{R}}_k^T \phi_k(\boldsymbol{X}_k) u_{1,k} d\tau \\ &\quad + \gamma \int_{t_0}^t s_k E_{s,k} d\tau + \gamma \int_{t_0}^t s_k \beta_{\varepsilon,k} u_{1,k} d\tau \\ &\quad + \gamma \int_{t_0}^t s_k \upsilon_k d\tau. \end{aligned} \tag{41}$$

Using the upper bound of υ_d and β_ε in (11) and (33), respectively, and (25), the following inequality is achieved:

$$\begin{aligned}\Delta V_k^{(2)} &\le -\frac{\gamma}{\lambda_2}\frac{s_{k-1}^2}{2} - \gamma\alpha_3 \int_{t_0}^t s_k^2 d\tau + \frac{\gamma}{\lambda_2}\frac{s_k^2(t_0)}{2} \\ &\quad + \bar{\upsilon}_d \gamma \int_{t_0}^t |s_k| d\tau + \gamma \int_{t_0}^t s_k \upsilon_k d\tau + \gamma \bar{\beta}_\epsilon \int_{t_0}^t |s_k| d\tau \\ &\quad + \gamma \int_{t_0}^t s_k \Psi_k \upsilon_{f_{1,k}} d\tau + \frac{4}{3}\alpha_2 \gamma \int_{t_0}^t |s_k| d\tau \\ &\quad + \gamma \int_{t_0}^t s_k E_{s,k} d\tau + \gamma \int_{t_0}^t s_k \widetilde{\boldsymbol{R}}_k^T \phi_k(\boldsymbol{X}_k) u_{1,k} d\tau. \end{aligned} \tag{42}$$

The difference of the third energy function between two successive iterations can be written as

$$\Delta V_k^{(3)} = \frac{1}{2b_q}\int_{t_0}^{t} \Psi_k^2 d\tau - \frac{1}{2b_q}\int_{t_0}^{t} \Psi_{k-1}^2 d\tau. \tag{43}$$

Based on (17) and [45], the following equation can be derived:

$$\begin{aligned}\frac{1}{2b_q}\left(\Psi_k^2 - \Psi_{k-1}^2\right) &= \frac{1}{2b_q}(\hat{\sigma}_k - \hat{\sigma}_{k-1})(\hat{\sigma}_k + \hat{\sigma}_{k-1} - 2\sigma) \\ &= \frac{1}{b_q}(\hat{\sigma}_k - \sigma)(\hat{\sigma}_k - \hat{\sigma}_{k-1}) \\ &\quad -\frac{1}{2b_q}(\hat{\sigma}_k - \hat{\sigma}_{k-1})(\hat{\sigma}_k - \hat{\sigma}_{k-1}).\end{aligned} \tag{44}$$

Considering (17), (44) can be rearranged as

$$\frac{1}{2b_q}\left(\Psi_k^2 - \Psi_{k-1}^2\right) = -\gamma\, \Psi_k s_k \upsilon_{f_{1,k}} - \frac{1}{2b_q}(\hat{\sigma}_k - \hat{\sigma}_{k-1})^2. \tag{45}$$

Therefore, $\Delta V_k^{(3)}$ in (43) can be simplified as

$$\begin{aligned}\Delta V_k^{(3)} &= -\frac{1}{2b_q}\int_{t_0}^{t} (\hat{\sigma}_k - \hat{\sigma}_{k-1})^2 d\tau \\ &\quad -\gamma \int_{t_0}^{t} \left(\Psi_k s_k \upsilon_{f_{1,k}}\right) d\tau.\end{aligned} \tag{46}$$

The difference of the fourth energy function between two iterations is

$$\Delta V_k^{(4)} = \frac{1}{2\xi}\int_{t_0}^{t} E_{s,k}^2 d\tau - \frac{1}{2\xi}\int_{t_0}^{t} E_{s,k-1}^2 d\tau. \tag{47}$$

Similarly, we can rewrite $\Delta V_k^{(4)}$ as

$$\begin{aligned}\frac{1}{2\xi}\left(E_{s,k}^2 - E_{s,k-1}^2\right) &= -\frac{1}{2\xi}\left(\hat{\upsilon}_{f_{2,k}} - \hat{\upsilon}_{f_{2,k-1}}\right)^2 \\ &\quad +\frac{1}{\xi}\left(\hat{\upsilon}_{f_{2,k}} - \upsilon_{f_{2,k}}\right)\left(\hat{\upsilon}_{f_{2,k}} - \hat{\upsilon}_{f_{2,k-1}}\right).\end{aligned} \tag{48}$$

Based on (26)–(28), we have

$$\frac{1}{2\xi}\left(E_{s,k}^2 - E_{s,k-1}^2\right) = -\gamma\, E_{s,k} s_k - \frac{1}{2\xi}\left(\hat{\upsilon}_{f_{2,k}} - \hat{\upsilon}_{f_{2,k-1}}\right)^2. \tag{49}$$

Hence,

$$\begin{aligned}\Delta V_k^{(4)} &= -\frac{1}{2\xi}\int_{t_0}^{t} \left(\hat{\upsilon}_{f_{2,k}} - \hat{\upsilon}_{f_{2,k-1}}\right)^2 d\tau \\ &\quad -\gamma \int_{t_0}^{t} \left(E_{s,k} s_k\right) d\tau.\end{aligned} \tag{50}$$

Considering $\widetilde{\boldsymbol{R}}_k(t_0) = 0$, the difference of the fifth energy function between two successive iterations can be written as

$$\Delta V_k^{(5)} = \frac{1}{2}tr\left\{\widetilde{\boldsymbol{R}}_k^T \widetilde{\boldsymbol{R}}_k\right\} - \frac{1}{2}tr\left\{\widetilde{\boldsymbol{R}}_{k-1}^T \widetilde{\boldsymbol{R}}_{k-1}\right\} \tag{51}$$

which can also be rewritten as

$$\Delta V_k^{(5)} = -tr\left\{\int_{t_0}^{t} \widetilde{R}_k^T \dot{\widetilde{R}}_k d\tau\right\} - \frac{1}{2}tr\left\{\widetilde{R}_{k-1}^T \widetilde{R}_{k-1}\right\}. \tag{52}$$

By substituting (30) into (51), $\Delta V_k^{(5)}$ can be obtained as

$$\begin{aligned}\Delta V_k^{(5)} &= -\frac{1}{2}tr\left\{\widetilde{\boldsymbol{R}}_{k-1}^T \widetilde{\boldsymbol{R}}_{k-1}\right\} \\ &\quad -tr\left\{\int_{t_0}^{t} \widetilde{\boldsymbol{R}}_k^T \left(\phi_k(\boldsymbol{X}_k) u_{1,k} s_k\right) d\tau\right\}.\end{aligned} \tag{53}$$

For proving the convergence of both the tracking error and s_k and removing unstable terms, consider $\gamma = \beta_1$, $\alpha_2 = -3(\bar{\upsilon}_d + \bar{\beta}_\varepsilon)/4$ and assume the values of $\bar{\upsilon}_d$ and $\bar{\beta}_\varepsilon$ are known. ΔV_k ultimately results in the following inequality:

$$\begin{aligned}\Delta V_k &= \Delta V_k^{(1)} + \Delta V_k^{(2)} + \Delta V_k^{(3)} + \Delta V_k^{(4)} + \Delta V_k^{(5)} \\ &\le -\frac{\upsilon_{k-1}^2}{2} - \frac{\gamma}{\lambda_2}\frac{s_{k-1}^2}{2} - \gamma\,\alpha_3 \int_{t_0}^{t} s_k^2 d\tau - \beta_2 \int_{t_0}^{t} \upsilon_k^2 d\tau \\ &\quad -\frac{1}{2b_q}\int_{t_0}^{t} (\hat{\sigma}_k - \hat{\sigma}_{k-1})^2 d\tau - \frac{1}{2\xi}\int_{t_0}^{t} \left(\hat{\upsilon}_{f_{2,k}} - \hat{\upsilon}_{f_{2,k-1}}\right)^2 d\tau \\ &\quad +\frac{\upsilon_k^2(t_0)}{2} + \frac{\gamma}{\lambda_2}\frac{s_k^2(t_0)}{2} - \frac{1}{2}tr\left\{\widetilde{\boldsymbol{R}}_{k-1}^T \widetilde{\boldsymbol{R}}_{k-1}\right\}.\end{aligned} \tag{54}$$

Equation (54) can be simplified further by choosing the gains $\beta_2 > 2$ and $\alpha_3 > 2/\lambda_2$ as

$$\begin{aligned}\Delta V_k &\le -\alpha_4 \int_{t_0}^{t} s_k^2 d\tau - \alpha_5 \int_{t_0}^{t} \upsilon_k^2 d\tau \\ &\quad -\frac{1}{2}tr\left\{\widetilde{\boldsymbol{R}}_{k-1}^T \widetilde{\boldsymbol{R}}_{k-1}\right\} - \frac{\upsilon_{k-1}^2}{2} - \frac{\gamma}{\lambda_2}\frac{s_{k-1}^2}{2} \\ &\quad -\frac{1}{2b_q}\int_{t_0}^{t} (\hat{\sigma}_k - \hat{\sigma}_{k-1})^2 d\tau - \frac{1}{2\xi}\int_{t_0}^{t} \left(\hat{\upsilon}_{f_{2,k}} - \hat{\upsilon}_{f_{2,k-1}}\right)^2 d\tau\end{aligned} \tag{55}$$

where $\alpha_4 \in \mathbb{R}^+$ and $\alpha_5 \in \mathbb{R}^+$. ΔV_k is negative semidefinite, which results in

$$V_k \le V_{k-1}, k = 1, 2, 3, \ldots \tag{56}$$

This demonstrates that V_k is a nonincreasing sequence. To prove the boundedness of V_k, using (20), (35), and (30), the time derivative of V_0 is derived below

$$\begin{aligned}\dot{V}_0 &= -\gamma\,\alpha_3 s_0^2 - \beta_2 \upsilon_0^2 + \frac{1}{b_q}\Psi_0^2 \\ &\quad +\gamma\, s_0 \Psi_0 \upsilon_{f_{1,0}} + \gamma\, s_0 E_{s,0} + \frac{1}{\xi}E_{s,0}^2.\end{aligned} \tag{57}$$

Based on (29) and (17), $\dot{V}_0$ can be further simplified as

$$\dot{V}_0 = -\gamma\,\alpha_3 s_k^2 - \beta_2 \upsilon_k^2 + \frac{1}{b_q}\sigma^2 + \frac{1}{\xi}\upsilon_{f_2}^2. \tag{58}$$

Therefore, $\dot{V}_0$ is bounded in the interval $[t_0, t]$, and V_0 is also bounded in $[t_0, t]$ because $V_0(t) = V_0(t_0) + \int_{t_0}^{t} \dot{V}_0(s) ds$.

It follows from (55) that V_k is bounded. Accordingly, υ_k, $\widetilde{\boldsymbol{R}}_k$, $\hat{\sigma}_k$,Ψ_k, $E_{s,k}$, and s_k are also bounded. Furthermore, based on (55), it can be shown that

$$\int_{t_0}^{t} s_k^2 d\tau \leq \frac{1}{\alpha_4}(V_{k-1} - V_k). \tag{59}$$

The fact that V_k is monotonically decreasing but is lower bounded by zero leads to the following conclusion:

$$\lim_{k\to\infty} \int_{t_0}^{t} s_k^2 d\tau = 0. \tag{60}$$

Based on (35) and considering (25), the boundedness of υ_k, $\widetilde{\boldsymbol{R}}_k$, $\hat{\sigma}_k$,Ψ_k, $E_{s,k}$, s_k, and $\dot{s}_k$ is also guaranteed. Accordingly, by applying the Barbalat-like lemma presented in [62] and [63], $\lim_{k\to\infty} s_k = 0$ uniformly on $[t_0, t]$. Using (18), this implies that $\bar{e}_1^{(i)}$ approaches zero with time. This further implies that the actual trajectories of subsystems ($\forall$ $i = 1, 2, \ldots, N$) will follow the desired movement profile defined in (4). Because $V_k(x, t)$ in (36) can be regarded as a common energy function in (34), it will be stable against arbitrary switching between different allocation coefficients (ι_n, ς_n) [64].

Remark 2: To implement this control method, the first step is to tune the control parameters. Understanding how the control parameters affect the performance of the closed-loop system is one of the important points for tuning. Here, several of the most important control parameters are mentioned. The speed of learning σ can be changed by b_q, the speed of learning Ω can be changed by changing the activation function gain, and the speed of learning $\upsilon_{f_2,k}$ can be changed by changing κ_1 and κ_2. The speed of learning must not be chosen to be so high that it causes noise accumulation and/or destabilizes the closed-loop control system.

Acknowledgment

The authors would like to thank A. Dodson for the assistance in the experimental test and K. Lambeth for the assistance in experiments and technical editing. The content is solely the responsibility of the authors and does not necessarily represent the official views of the National Institutes of Health. Any recommendations, opinions, conclusions, and findings expressed in this material are those of the author(s) and do not necessarily reflect the National Science Foundation views.

References

[1] A. Kantrowitz, "Electronic physiologic aids," *Rep. Maimonides Hospital*, pp. 4–5, Apr. 1960.

[2] W. Liberson, H. Holmquest, D. Scot, and M. Dow, "Functional electrotherapy: Stimulation of the peroneal nerve synchronized with the swing phase of the gait of hemiplegic patients," *Arch. Phys. Med*, vol. 42, pp. 101–105, May 1961.

[3] V. Nekoukar and A. Erfanian, "A decentralized modular control framework for robust control of FES-activated Walker-assisted paraplegic walking using terminal sliding mode and fuzzy logic control," *IEEE Trans. Biomed. Eng.*, vol. 59, no. 10, pp. 2818–2827, Oct. 2012.

[4] C. E. King, P. T. Wang, C. M. McCrimmon, C. C. Chou, A. H. Do, and Z. Nenadic, "The feasibility of a brain-computer interface functional electrical stimulation system for the restoration of overground walking after paraplegia," *J. Neuroeng. Rehabil.*, vol. 12, no. 1, p. 80, Dec. 2015.

[5] M. Bijak *et al.*, "Stimulation parameter optimization for FES supported standing up and walking in SCI patients," *Artif. Organs*, vol. 29, no. 3, pp. 220–223, Mar. 2005.

[6] M. S. Poboroniuc, D. E. Wood, R. Riener, and N. N. Donaldson, "A new controller for FES-assisted sitting down in paraplegia," *Adv. Electr. Comput. Eng.*, vol. 10, no. 4, pp. 9–16, 2010.

[7] K.-S. Jung, T.-S. In, and H.-Y. Cho, "Effects of sit-to-stand training combined with transcutaneous electrical stimulation on spasticity, muscle strength and balance ability in patients with stroke: A randomized controlled study," *Gait Posture*, vol. 54, pp. 183–187, May 2017.

[8] J. B. Lee, S. B. Kim, K. W. Lee, J. H. Lee, J. G. Park, and S. J. Lee, "Combined therapy with functional electrical stimulation and standing frame in stroke patients," *Ann. Rehabil. Med.*, vol. 43, no. 1, p. 96, 2019.

[9] M. O. Ibitoye, N. A. Hamzaid, M. Hayashibe, N. Hasnan, and G. M. Davis, "Restoring prolonged standing via functional electrical stimulation after spinal cord injury: A systematic review of control strategies," *Biomed. Signal Process. Control*, vol. 49, pp. 34–47, Mar. 2019.

[10] M. K. Nagai, C. Marquez-Chin, and M. R. Popovic, "Why is functional electrical stimulation therapy capable of restoring motor function following severe injury to the central nervous system?" in *Translational Neuroscience*. Boston, MA, USA: Springer, 2016, pp. 479–498.

[11] P. H. Peckham and J. S. Knutson, "Functional electrical stimulation for neuromuscular applications," *Annu. Rev. Biomed. Eng.*, vol. 7, no. 1, pp. 327–360, Aug. 2005.

[12] D. F. P. Granados, H. Kadone, and K. Suzuki, "Unpowered lower-body exoskeleton with torso lifting mechanism for supporting sit-to-stand transitions," in *Proc. IEEE/RSJ Int. Conf. Intell. Robots Syst. (IROS)*, Oct. 2018, pp. 2755–2761.

[13] H.-F. Mao, H.-P. Huang, T.-W. Lu, T.-M. Wang, C.-H. Wu, and J.-S. Hu, "Balance control and energetics of powered exoskeleton-assisted sit-to-stand movement in individuals with paraplegic spinal cord injury," *Arch. Phys. Med. Rehabil.*, vol. 99, no. 10, pp. 1982–1990, Oct. 2018.

[14] K. Sasaki, M. Sugimoto, T. Sugiyama, D. F. Paez Granados, and K. Suzuki, "Child-sized passive exoskeleton for supporting voluntary sitting and standing motions," in *Proc. IEEE/RSJ Int. Conf. Intell. Robots Syst. (IROS)*, Oct. 2018, pp. 5457–5462.

[15] O. Narvaez Aroche, P.-J. Meyer, S. Tu, A. Packard, and M. Arcak, "Robust control of the sit-to-stand movement for a powered lower limb orthosis," *IEEE Trans. Control Syst. Technol.*, vol. 28, no. 6, pp. 2390–2403, Nov. 2020.

[16] H. Zheng, T. Shen, M. R. Afsar, I. Kang, A. J. Young, and X. Shen, "A semi-wearable robotic device for sit-to-stand assistance," in *Proc. IEEE 16th Int. Conf. Rehabil. Robot. (ICORR)*, Jun. 2019, pp. 204–209.

[17] J. Vantilt *et al.*, "Model-based control for exoskeletons with series elastic actuators evaluated on sit-to-stand movements," *J. Neuroeng. Rehabil.*, vol. 16, no. 1, p. 65, Dec. 2019.

[18] A. J. Del-Ama, A. D. Koutsou, J. C. Moreno, A. De-Los-Reyes, A. Gil-Agudo, and J. L. Pons, "Review of hybrid exoskeletons to restore gait following spinal cord injury," *J. Rehabil. Res. Develop.*, vol. 49, no. 4, pp. 497–514, 2012.

[19] A. J. del-Ama, Á. Gil-Agudo, J. L. Pons, and J. C. Moreno, "Hybrid FES-robot cooperative control of ambulatory gait rehabilitation exoskeleton," *J. Neuroeng. Rehabil.*, vol. 11, no. 1, p. 27, 2014.

[20] N. A. Kirsch, X. Bao, N. A. Alibeji, B. E. Dicianno, and N. Sharma, "Model-based dynamic control allocation in a hybrid neuroprosthesis," *IEEE Trans. Neural Syst. Rehabil. Eng.*, vol. 26, no. 1, pp. 224–232, Jan. 2018.

[21] K. H. Ha, S. A. Murray, and M. Goldfarb, "An approach for the cooperative control of FES with a powered exoskeleton during level walking for persons with paraplegia," *IEEE Trans. Neural Syst. Rehabil. Eng.*, vol. 24, no. 4, pp. 455–466, Apr. 2016.

[22] N. Alibeji, N. Kirsch, and N. Sharma, "An adaptive low-dimensional control to compensate for actuator redundancy and FES-induced muscle fatigue in a hybrid neuroprosthesis," *Control Eng. Pract.*, vol. 59, pp. 204–219, Feb. 2017.

[23] N. A. Alibeji, N. A. Kirsch, and N. Sharma, "A muscle synergy-inspired adaptive control scheme for a hybrid walking neuroprosthesis," *Frontiers Bioeng. Biotechnol.*, vol. 3, p. 203, Dec. 2015.

[24] N. A. Alibeji, V. Molazadeh, F. Moore-Clingenpeel, and N. Sharma, "A muscle synergy-inspired control design to coordinate functional electrical stimulation and a powered exoskeleton: Artificial generation of synergies to reduce input dimensionality," *IEEE Control Syst.*, vol. 38, no. 6, pp. 35–60, Dec. 2018.

[25] O. Harib *et al.*, "Feedback control of an exoskeleton for paraplegics: Toward robustly stable, hands-free dynamic walking," *IEEE Control Syst.*, vol. 38, no. 6, pp. 61–87, Dec. 2018.

[26] M. A. Alouane, W. Huo, H. Rifai, Y. Amirat, and S. Mohammed, "Hybrid FES-exoskeleton controller to assist sit-to-stand movement," *IFAC-PapersOnLine*, vol. 51, no. 34, pp. 296–301, 2019.

[27] N. A. Alibeji, V. Molazadeh, B. E. Dicianno, and N. Sharma, "A control scheme that uses dynamic postural synergies to coordinate a hybrid walking neuroprosthesis: Theory and experiments," *Frontiers Neurosci.*, vol. 12, p. 159, Apr. 2018.

[28] J. W. Grizzle, G. Abba, and F. Plestan, "Asymptotically stable walking for biped robots: Analysis via systems with impulse effects," *IEEE Trans. Autom. Control*, vol. 46, no. 1, pp. 51–64, Jan. 2001.

[29] E. R. Westervelt, J. W. Grizzle, C. Chevallereau, J. H. Choi, and B. Morris, *Feedback Control of Dynamic Bipedal Robot Locomotion*, vol. 28. Boca Raton, FL, USA: CRC Press, 2007.

[30] R. D. Gregg and J. W. Sensinger, "Towards biomimetic virtual constraint control of a powered prosthetic leg," *IEEE Trans. Control Syst. Technol.*, vol. 22, no. 1, pp. 246–254, Jan. 2014.

[31] T. Gurriet *et al.*, "Towards restoring locomotion for paraplegics: Realizing dynamically stable walking on exoskeletons," in *Proc. IEEE Int. Conf. Robot. Autom. (ICRA)*, May 2018, pp. 2804–2811.

[32] M. E. Mungai and J. W. Grizzle, "Feedback control design for robust comfortable sit-to-stand motions of 3D lower-limb exoskeletons," *IEEE Access*, vol. 9, pp. 122–161, 2021.

[33] V. Ghanbari, V. H. Duenas, P. J. Antsaklis, and W. E. Dixon, "Passivity-based iterative learning control for cycling induced by functional electrical stimulation with electric motor assistance," *IEEE Trans. Control Syst. Technol.*, vol. 27, no. 5, pp. 2287–2294, Sep. 2019.

[34] J. Bae and M. Tomizuka, "A gait rehabilitation strategy inspired by an iterative learning algorithm," *Mechatronics*, vol. 22, no. 2, pp. 213–221, Mar. 2012.

[35] P. Sampson *et al.*, "Using functional electrical stimulation mediated by iterative learning control and robotics to improve arm movement for people with multiple sclerosis," *IEEE Trans. Neural Syst. Rehabil. Eng.*, vol. 24, no. 2, pp. 235–248, Feb. 2016.

[36] N. Sharma, C. M. Gregory, M. Johnson, and W. E. Dixon, "Closed-loop neural network-based NMES control for human limb tracking," *IEEE Trans. Control Syst. Technol.*, vol. 20, no. 3, pp. 712–725, May 2012.

[37] F. L. Lewis, R. Selmic, and J. Campos, *Neuro-Fuzzy Control of Industrial Systems With Actuator Nonlinearities*. Philadelphia, PA, USA: SIAM, 2002.

[38] V. Molazadeh, Z. Sheng, X. Bao, and N. Sharma, "A robust iterative learning switching controller for following virtual constraints: Application to a hybrid neuroprosthesis," in *Proc. CPHS*, 2018, pp. 28–33.

[39] V. Molazadeh, Z. Sheng, X. Bao, and N. Sharma, "A robust iterative learning switching controller for following virtual constraints: Application to a hybrid neuroprosthesis," *IFAC-PapersOnLine*, vol. 51, no. 34, pp. 28–33, 2019.

[40] Y. Marinakis and M. Marinaki, "A hybrid genetic–particle swarm optimization algorithm for the vehicle routing problem," *Expert Syst. Appl.*, vol. 37, no. 2, pp. 1446–1455, 2010.

[41] M. Chen, S. Sam Ge, and B. How, "Robust adaptive neural network control for a class of uncertain MIMO nonlinear systems with input nonlinearities," *IEEE Trans. Neural Netw.*, vol. 21, no. 5, pp. 796–812, May 2010.

[42] N. Alibeji, B. E. Dicianno, and N. Sharma, "Bilateral control of functional electrical stimulation and robotics-based telerehabilitation," *Int. J. Intell. Robot. Appl.*, vol. 1, no. 1, pp. 6–18, Feb. 2017.

[43] T. Schauer *et al.*, "Online identification and nonlinear control of the electrically stimulated quadriceps muscle," *Control Eng. Pract.*, vol. 13, no. 9, pp. 1207–1219, Sep. 2005.

[44] N. Sharma, N. A. Kirsch, N. A. Alibeji, and W. E. Dixon, "A non-linear control method to compensate for muscle fatigue during neuromuscular electrical stimulation," *Frontiers Robot. AI*, vol. 4, p. 68, Dec. 2017.

[45] W. Chen, Y.-Q. Chen, and C.-P. Yeh, "Robust iterative learning control via continuous sliding-mode technique with validation on an SRV02 rotary plant," *Mechatronics*, vol. 22, no. 5, pp. 588–593, Aug. 2012.

[46] A. Kralj and T. Bajd, *Functional Electrical Stimulation: Standing and Walking After Spinal Cord Injury*. Boca Raton, FL, USA: CRC Press, 1989.

[47] R. B. Stein, E. P. Zehr, M. K. Lebiedowska, D. B. Popovic, A. Scheiner, and H. J. Chizeck, "Estimating mechanical parameters of leg segments in individuals with and without physical disabilities," *IEEE Trans. Rehabil. Eng.*, vol. 4, no. 3, pp. 201–211, Sep. 1996.

[48] N. Sharma, C. M. Gregory, and W. E. Dixon, "Predictor-based compensation for electromechanical delay during neuromuscular electrical stimulation," *IEEE Trans. Neural Syst. Rehabil. Eng.*, vol. 19, no. 6, pp. 601–611, Dec. 2011.

[49] N. Sharma, K. Stegath, C. M. Gregory, and W. E. Dixon, "Nonlinear neuromuscular electrical stimulation tracking control of a human limb," *IEEE Trans. Neural Syst. Rehabil. Eng.*, vol. 17, no. 6, pp. 576–584, Dec. 2009.

[50] J. J. Abbas and H. J. Chizeck, "Neural network control of functional neuromuscular stimulation systems: Computer simulation studies," *IEEE Trans. Biomed. Eng.*, vol. 42, no. 11, pp. 1117–1127, Nov. 1995.

[51] A. Ajoudani and A. Erfanian, "A neuro-sliding-mode control with adaptive modeling of uncertainty for control of movement in paralyzed limbs using functional electrical stimulation," *IEEE Trans. Biomed. Eng.*, vol. 56, no. 7, pp. 1771–1780, Jul. 2009.

[52] J. Riess and J. J. Abbas, "Adaptive neural network control of cyclic movements using functional neuromuscular stimulation," *IEEE Trans. Rehabil. Eng.*, vol. 8, no. 1, pp. 42–52, Mar. 2000.

[53] M. Kutlu, C. Freeman, A.-M. Hughes, and M. Spraggs, "A home-based FES system for upper-limb stroke rehabilitation with iterative learning control," *IFAC-PapersOnLine*, vol. 50, no. 1, pp. 12089–12094, Jul. 2017.

[54] J. Zhang, C. C. Cheah, and S. H. Collins, "Experimental comparison of torque control methods on an ankle exoskeleton during human walking," in *Proc. IEEE Int. Conf. Robot. Autom. (ICRA)*, May 2015, pp. 5584–5589.

[55] C. A. Rouse, R. J. Downey, C. M. Gregory, C. A. Cousin, V. H. Duenas, and W. E. Dixon, "FES cycling in stroke: Novel closed-loop algorithm accommodates differences in functional impairments," *IEEE Trans. Biomed. Eng.*, vol. 67, no. 3, pp. 738–749, Mar. 2020.

[56] C. A. Cousin *et al.*, "Closed-loop cadence and instantaneous power control on a motorized functional electrical stimulation cycle," *IEEE Trans. Control Syst. Technol.*, vol. 28, no. 6, pp. 2276–2291, Nov. 2020.

[57] C. A. Cousin, C. A. Rouse, V. H. Duenas, and W. E. Dixon, "Controlling the cadence and admittance of a functional electrical stimulation cycle," *IEEE Trans. Neural Syst. Rehabil. Eng.*, vol. 27, no. 6, pp. 1181–1192, Jun. 2019.

[58] B. Chen *et al.*, "Sit-to-stand and stand-to-sit assistance for paraplegic patients with CUHK-EXO exoskeleton," *Robotica*, vol. 36, no. 4, p. 535, 2018.

[59] A. Tsukahara, R. Kawanishi, Y. Hasegawa, and Y. Sankai, "Sit-to-stand and stand-to-sit transfer support for complete paraplegic patients with robot suit HAL," *Adv. Robot.*, vol. 24, no. 11, pp. 1615–1638, Jan. 2010.

[60] W. Huo, S. Mohammed, Y. Amirat, and K. Kong, "Active impedance control of a lower limb exoskeleton to assist sit-to-stand movement," in *Proc. IEEE Int. Conf. Robot. Autom. (ICRA)*, May 2016, pp. 3530–3536.

[61] S. Jatsun, S. Savin, A. Yatsun, and R. Turlapov, "Adaptive control system for exoskeleton performing sit-to-stand motion," in *Proc. 10th Int. Symp. Mechatronics Appl. (ISMA)*, Dec. 2015, pp. 1–6.

[62] J.-X. Xu, Y. Tan, and T.-H. Lee, "Iterative learning control design based on composite energy function with input saturation," *Automatica*, vol. 40, no. 8, pp. 1371–1377, Aug. 2004.

[63] M. Sun, "A barbalat-like lemma with its application to learning control," *IEEE Trans. Autom. Control*, vol. 54, no. 9, pp. 2222–2225, Sep. 2009.

[64] D. Liberzon, *Switching in Systems and Control*. Basel, Switzerland: Birkhäuser, 2003.